SEDIMENTOLOGY the journal of the International Association of Sedimentologists

Sedimentology (2021) **68**, 1297–1327 doi: 10.1111/sed.12860

Three-dimensional submerged wall jets and their transition to density flows: Morphodynamics and implications for the depositional record

JÖRG LANG*, JUAN J. FEDELE† and DAVID C. J. D. HOYAL†
**Institut für Geologie, Leibniz Universität Hannover, Callinstraße 30, Hannover, 30167, Germany (E-mail: lang@geowi.uni-hannover.de)*
†ExxonMobil Upstream Research Company, 22777 Springwood Village Parkway, Spring, TX, 77389, USA

Associate Editor – Matthieu Cartigny

ABSTRACT

Jets that expand from an orifice into an ambient water body represent a basic flow model for depositional environments related to expanding flows. Momentum-dominated jets evolve into gravity-dominated density flows. To understand this transition and its sedimentological relevance, three-dimensional tank experiments with submerged wall jets were conducted, systematically varying parameters such as the initial density difference, bed slope, grain size and sediment supply. Bedform successions could be subdivided into those related to the jet and those related to the density flow. Jet deposits included early-stage bedforms, scours and mouth bars. Early-stage bedforms are asymmetrical dunes that spread concentrically from the orifice. Sediment entrainment by eddies from the expanding jets led to the formation of scours and mouth bars. Flows with lesser initial density difference produced more elongate scours. Conversely, scours became deeper for denser incoming flows. Coarser-grained sediment caused the formation of higher and steeper mouth bars and vice versa. The transition from momentum-dominated jets to gravity-dominated density flows occurred approximately at the mouth-bar crest. Hydraulic jumps were absent in the expanding jet regions and at the transitions to density flows. Instead, complex flow patterns and circulations were inferred from the velocity measurements within the scour and at the mouth-bar crests. Bedform trains related to the density flow were controlled by the grain size and sediment supply. Coarse-grained sediment and high supply rates caused strong mouth-bar aggradation and flow splitting, leading to the formation of bedform trains laterally adjacent to the mouth bar. Fine-grained sediment and low supply rates caused the formation of bedform trains downflow of the mouth bar. The symmetrical bedforms deposited by the density flows always displayed an in-phase relationship with the flow, indicating that they were antidunes. The experimental jet deposits resemble successions known from subaqueous ice-contact fans and deep water channel-lobe transition zones.

Keywords Channel-lobe transition zone, density flow, hydraulic jump, subaqueous ice-contact fan, supercritical flow, wall jet.

INTRODUCTION

Three-dimensional jets are flows that emerge from an orifice into an ambient water body and decelerate and expand due to the entrainment of the ambient water (Fig. 1A to D). At the orifice, jets are typically momentum-dominated and evolve into more gravity-dominated flows by dissipation of the initial momentum (Bates, 1953; List, 1982; Powell, 1990). Jet-like behaviour characterizes all kinds of expanding flows, and jets are therefore considered as a basic flow model for clastic deposition in a variety of depositional environments (Bates, 1953; Powell, 1990; Hoyal *et al.,* 2003; Hamilton *et al.,* 2017). Examples of depositional environments that can be modelled as point-sourced jets include deltas (Bates, 1953; Wright, 1977; Wellner *et al.,* 2005; Ahmed *et al.,* 2014; Fidolini & Ghinassi, 2016; Daniller-Varghese *et al.,* 2020), submarine fans (Beaubouef *et al.,* 2003; Alexander *et al.,* 2008; Terlaky & Arnott, 2014; Terlaky *et al.,* 2016) and subaqueous ice-contact fans (Powell, 1990; Russell & Arnott, 2003; Hornung *et al.,* 2007; Winsemann *et al.,* 2009; Lang & Winsemann, 2013; Dowdeswell *et al.,* 2015; Aquino *et al.,* 2016; Lang *et al.,* 2017, 2020). Jets and their deposits display a distinct proximal (near-field) to distal (far-field) zonation, reflecting the spatial evolution of the initial jet. The deceleration of the flow is reflected by downflow and lateral grain-size decay. Bedform successions pass from a region of bypass and erosion via a region of bedform formation into a region of suspension settling (Powell, 1990; Hoyal *et al.,* 2003; Russell & Arnott, 2003; Winsemann *et al.,* 2009; Lang *et al.,* 2017). Momentum-dominated jets evolve into subcritical or supercritical gravity-dominated density flows in the far-field regions after jet momentum has dissipated (Fig. 1A to D). The evolution from jets into density flows is primarily controlled by the initial momentum, the density difference between the flow and the ambient water and the bed slope (Powell, 1990; Hoyal *et al.,* 2003). However, the transition between the jet and density flow endmembers is not well-understood, particularly in wall jets (Chu & Baddour, 1984; Hoyal *et al.,* 2003). Several previous sedimentological studies suggested the occurrence of hydraulic jumps at the transition from supercritical jets to subcritical density flows (Russell & Arnott, 2003; Hornung *et al.,* 2007; Winsemann *et al.,* 2009; Lang & Winsemann, 2013; Terlaky & Arnott, 2014). These interpretations were inspired by two-dimensional flume studies, where hydraulic jumps are common (e.g. Rajaratman & Subramanyam, 1986; Long *et al.,* 1990). Hydraulic jumps are fundamental localized flow features with important implications for morphodynamics and deposition in supercritical density flows (e.g. Hamilton *et al.,* 2015, 2017), while qualitative observations from experiments with three-dimensional wall jets suggest that hydraulic jumps are very weak or absent (Hoyal *et al.,* 2003).

The aim of this study is to improve the understanding of the morphodynamics of jets, associated gravity-dominated flows and their deposits. Tank experiments with three-dimensional submerged wall jets were conducted, systematically varying the main controlling factors such as the initial density difference with the ambient water, sediment grain size, sediment supply and bed slope, to answer several key questions:

- What are the characteristic fluid and sediment-transport dynamics of submerged wall jets under different conditions?
- How do momentum-dominated wall jets transit into gravity-dominated density flows? Is there a hydraulic jump involved? How is this transition affected by erosion and deposition?
- Can wall jets be used as an analogue for the flow dynamics of expanding density flows? What are the implications to infer flow dynamics from the depositional record of expanding flows?

In this study, experimental results are presented that link the hydrodynamics of jets and associated gravity-dominated density flows to their corresponding deposits, characteristic sedimentological features and morphodynamic evolution in both the near-field and far-field regions. Stratified jets were created by saline and saline-sediment suspensions in the initial efflux and were acting on horizontal or sloping sediment beds. A series of base-line experiments including non-stratified (pure) 3D jets expanding onto horizontal, fixed beds were also performed to test, verify and compare results related to flow dynamics and evolution. New observations are reported on: (i) the effects of initial density on scour geometry; (ii) the absence of hydraulic jumps; (iii) the effects of grain-size and lee-side gradient of the mouth bar; (iv) distinctive bedforms; and (v) the characteristic hydraulic regimes in the distal, density-flow controlled far-field regions.

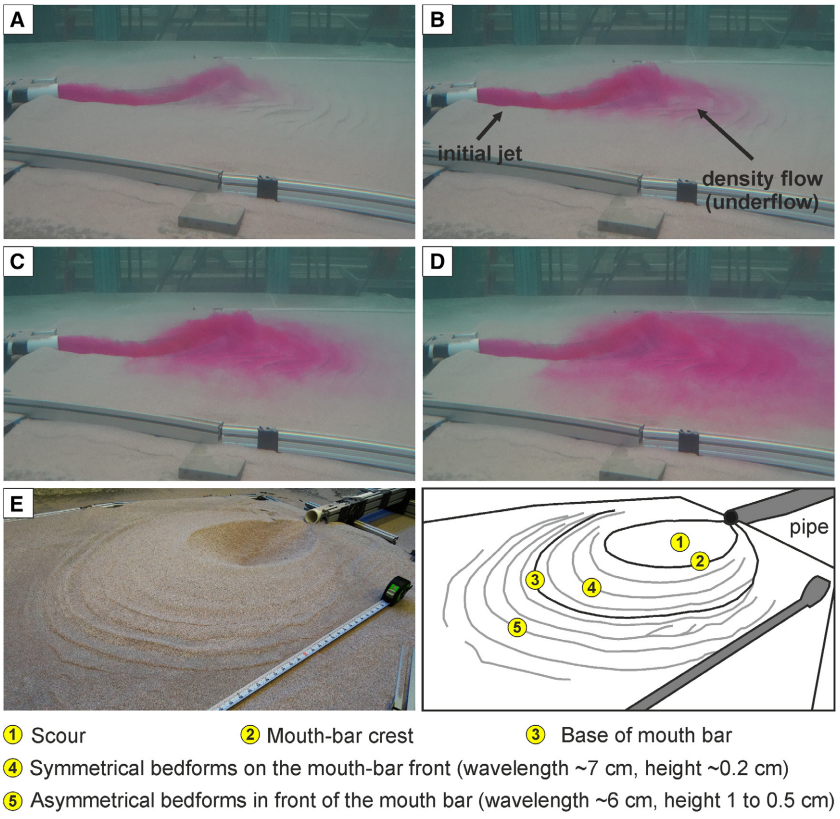

Fig. 1. (A) to (D) Photographs from a typical experimental jet (densimetric Froude number $Fr' = 4.02$; horizontal bed). (A) The jet expands and decelerates within the scour. (B) The decelerated flow ('plume') is pushed over the mouth bar by the incoming jet. (C) A density flow (underflow) forms on the distal side of the mouth bar. (D) The density flow spreads downflow and laterally from the mouth bar. (E) Oblique photograph and line drawing of a typical jet deposit to illustrate the characteristic features (densimetric Froude number $Fr' = 2.08$; horizontal medium-grained sediment bed; sediment-supply rate 2.2 g s^{-1}).

JETS AND THEIR DEPOSITS

Jets expand from an orifice into an ambient water body and evolve downflow from a momentum-dominated jet into a gravity-dominated density flow (Fig. 1A to D). Deceleration and expansion are controlled by the exchange of fluid and momentum due to the generation of turbulent eddies at the free boundaries of the jet (Tollmien, 1926; Wright, 1977; List, 1982). This downflow evolution is commonly referred to as jet-plume pair (Powell, 1990; Hoyal *et al.,* 2003). Stratified jets (also termed buoyant) have an initial density difference in relation to the ambient water due to temperature, salinity or suspended sediments and might be capable of evolving into gravity-dominated flows, particularly in cases of a positive density difference (i.e. efflux denser than ambient water), in the far-field. In contrast, pure (also termed non-stratified) jets are homopycnal flows that have the same density as the ambient water and will not evolve into a gravity-dominated flow in the far-field (distal) regions. The basic dynamics of three-dimensionally expanding jets, and thus their sedimentological behaviour, might differ substantially when compared with simpler, laterally confined (2D) jets. Lateral confinement increases the turbulent boundary shear and thus the impact of friction (Launder & Rodi, 1983). Submerged, expanding (3D) wall jets are in contact with the basin floor and thus subject to deceleration due to basal friction (Fig. 1A; Wright, 1977; Powell, 1990). In these cases, the lateral expansion is always larger than the vertical expansion (ratio 5 : 1 to 8 : 1; Launder & Rodi, 1983).

The maximum flow velocity occurs at the outlet of a (typically pressurized) flow (orifice), where the efflux of momentum and buoyancy takes place. Natural jets are considered fully turbulent whenever the Reynolds number (Re) based on the efflux velocity, orifice diameter and kinematic viscosity of the source fluid is larger than about 2×10^3 (Rajaratnam & Berry, 1977; Launder & Rodi, 1983; Powell, 1990; Jirka, 2004). Mixing and turbulence can be reduced greatly due to stratification (Ellison & Turner, 1959; Fischer *et al.,* 1979; Turner, 1986).

The densimetric Froude number Fr' has often been used to describe the degree of stratification at the outlet. It is given by $Fr' = \bar{u}/\sqrt{(g' d)}$, where $\bar{u}$ is the efflux mean flow velocity, d is the

orifice diameter, and g' is the reduced gravity defined by $g' = g\,(\rho_f - \rho_w)/\rho_f$, with ρ_f as the density of the inflow and ρ_w as the density of the receiving ambient water. An alternative expression for characterizing stratification at the outflow is the bulk Richardson number (Powell, 1990) which is defined as $Ri = g'\,d/\bar{u}^2$, or as readily seen, $Ri = 1/Fr'^2$.

Stratified jets are common in natural environments and in many engineering applications. Because of the wide variety of possibilities of jet and ambient flow and density interactions, the flow complexities and physical processes involved are vast. This is clearly reflected in the extensive amount of work published dealing with different basic settings of flow configuration, varying approaches for investigation and specific nomenclature and definitions proposed for some of the governing dimensionless parameters [see Jirka (2004) for a comprehensive summary of the historical development]. This study is concentrated on wall jets that have a positive density difference (i.e. denser) with respect to the receiving water body at the efflux location, discharging parallel to an existing loose-sediment bed. Because of the nature of this specific setting, the densimetric Froude number has been proposed as a means to evaluate the relative importance of inertial versus gravitational forces, in analogy to open-channel or density flows (Rajaratnam & Berry, 1977; Hoyal *et al.,* 2003). While this latter dynamic interpretation of the densimetric Froude number might apply after the jets transition to gravity-dominated density flows in the far-field, it might not be applicable in the near-field region, where momentum-dominated flows with particular turbulence properties and complex flow interactions and transitions are not boundary-layer like, lacking a proper flow interface, characteristic force balances or turbulence invariance. Thus, the dynamic characterization of near-field jet regions (momentum-dominated) as supercritical or subcritical might not be appropriate because the flows do not resemble gravity-dominated flows with an interface. However, the densimetric Froude number represents a parameter to conveniently characterize the initial flow conditions at the orifice with respect to the discharge, flow velocity, orifice diameter and excess flow density.

Seminal theoretical studies have used input mass, momentum and density flux parameters to characterize the proximal jet regions (Baines, 1995, 2002), but some studies have proposed empirically-derived values of the densimetric Froude to describe limiting conditions between momentum versus gravity control: $Fr' \geq 1.3$ for axisymmetrical jets and $Fr' \geq 1.2$ for wall jets (corresponding to $Ri' \leq 0.56$ for axisymmetrical jets and $Ri' \leq 0.735$ for wall jets), respectively (List, 1982; Powell, 1990; Roberts *et al.,* 2001). Further controlling factors proposed for describing these flow transitions include sediment concentration, grain size, and the density difference between the fluid and the sediment (Bates, 1953; Powell, 1990; Chiew & Lim, 1996; Hoyal *et al.,* 2003).

Previous wall-jet studies have described a proximal to distal zonation that includes: (i) the zone of flow establishment (ZFE); (ii) the zone of flow transition (ZFT); and (iii) the zone of established flow (ZEF; Bates, 1953; Fischer *et al.,* 1979; List, 1982; Powell, 1990). The ZFE is characterized by a constant velocity of the jet core, corresponding to the velocity at the orifice. In the ZFT the core velocity decreases with a constant rate of deceleration. In the ZEF, the axial velocity decreases rapidly to a negligible value and turbulent mixing takes place throughout the entire flow. The downflow extent of the different zones scales with the orifice diameter and is modified by boundary friction (Powell, 1990).

The evolution from jets to density flows is primarily controlled by the initial momentum and the density contrast. This flow evolution is also referred to as the near-field and far-field of a jet. The near-field is the region where inertia and mixing processes are controlled by the discharge parameters at the orifice (Roberts *et al.,* 2001). It is commonly assumed that density contrasts have a limited effect on flow structure and morphodynamics in the near-field. However, in this study a strong effect of the initial density difference on the final configuration of the scour was observed. At the transition to the far-field, the effect of density differences becomes increasingly important as inertia decays and the flow evolves into a gravity-dominated density flow. The end of the near-field is characterized by the collapse of discharge-induced turbulence under the influence of gravity forces (Roberts *et al.,* 2001). In the far-field, the decelerated jet has fully evolved into a density flow and is controlled by gravity and buoyancy forces. If the flow is denser than the ambient water, it evolves into a dense underflow (Powell, 1990). Gravity-dominated density flows are free to interact with the slope, the substratum, the ambient fluid and

lateral confinement. The behaviour of free density flows is characterized by the bed slope, the flow density, the size of suspended sediment and the bottom friction (Cantelli *et al.,* 2011; Sequeiros, 2012; Fernandez *et al.,* 2014; Hamilton *et al.,* 2015).

Sedimentary features associated with submerged wall jets are typically characterized by a scour–mouth bar pair (Fig. 1E). The geometries of the scour and associated mouth bar have also been linked to the densimetric Froude number (Bates, 1953; Powell, 1990; Chiew & Lim, 1996; Ade & Rajaratnam, 1998; Hoyal *et al.,* 2003; Baas *et al.,* 2004; Alexander *et al.,* 2008). The downflow bedform successions reflect the spatial deceleration and temporal evolution of the jet, from bypass and erosion via bedform formation to suspension settling (Powell, 1990; Russell & Arnott, 2003; Hornung *et al.,* 2007; Winsemann *et al.,* 2009; Lang & Winsemann, 2013; Lang *et al.,* 2017, 2020). Distally, the evolution of the deposits is closely related to the density contrast with the ambient water (Powell, 1990) and topographic gradient, as flows might have turned into gravity-dominated density flows, thus transporting sediments farther into the basin. Sediment settling due to decreasing jet-related turbulence may further contribute to the development of density flows (Powell, 1990; Strom & Keyvani, 2011; Dowdeswell *et al.,* 2015).

The cases investigated in this study include both pure (no density difference with ambient water) or stratified (due to salinity, sediment in suspension, or both) wall jets impinging on an existing sediment bed, with or without gradient. In addition, a few base cases in which horizontal, fixed beds were used are reported here as well. In all cases, the characteristic jet zonation and evolution were observed and described in dynamic terms, aided by measurements of velocity and density distributions. Not only did the hydrodynamics in each of the cases show characteristic evolution and zonation, but the nature and evolution of the resulting associated deposits are also closely linked.

METHODS

Set-up of the experiments

Three-dimensional tank experiments with submerged wall jets and density flows were conducted in the Sedimentology and Stratigraphy Experimental Facility at ExxonMobil Upstream Research Company (Houston, Texas, USA). The experimental domain comprises an 8 m long and 5 m wide plate that is placed in a 10 m long, 7 m wide and 2 m deep glass-walled tank filled with tap water (Fig. 2). The slope of the plate is adjustable, and both horizontal and inclined configurations were used in the experiments. A system comprising a Venturi pipe and external feeder for sediment or salt is used to combine desired water discharge rates and sediment or salt discharge rates. Water, salt and sediment are mixed through the Venturi pipe and pumped to a head tank. This system provides the capability of steady, long duration flows.

Jets were released from pipes with diameters of 2.54 or 5.08 cm, respectively, mounted to the plate either directly adjacent to the bare metal (fixed bed runs) or overlying a constant thickness bed of sediment (mobile bed runs). Accordingly, the axis of the pipe was half the pipe diameter above the surface of the bed. The water depth above the outlet of the pipe was approximately 0.8 to 1.0 m to generate fully submerged jets, not interfering with the water surface. Flow discharge and pipe diameter were selected to move and deposit the sediment size used in the experiment, allowing for convenient and detailed observations of the flow characteristics and the resulting bed topography. The set-up included slow feed of freshwater and slow drain of the accumulated denser fluid from the bottom of the tank during the runs. The additional tank storage volume at the downflow end and lateral sides prevented build-up of stratified fluid to the level of the outflow at the end of the plate.

Stratified, dense jets were produced using a brine solution of constant density by mixing water and salt in the Venturi in-line mixing system, while for experiments with pure jets (non-stratified) no salt was added. A variety of sediment sizes was used either for creating the beds in the tank, or for feeding into the Venturi mixing system, thus entering the tank in suspension through the jets. The sediment used in the experiments is a crushed melamine plastic with a density of 1.57 g cm^{-3}, which is supplied in sieved uniform mixtures of fine (0.149 to 0.177 mm), medium (0.177 to 0.25 mm), coarse (0.25 to 0.42 mm) and very coarse (0.59 to 0.84 mm) grains. The choice of the material was checked with a Shield's number scaling, where the ratio of flow-imposed shear to mechanical properties of the sediment (i.e. size and submerged specific gravity) were roughly estimated

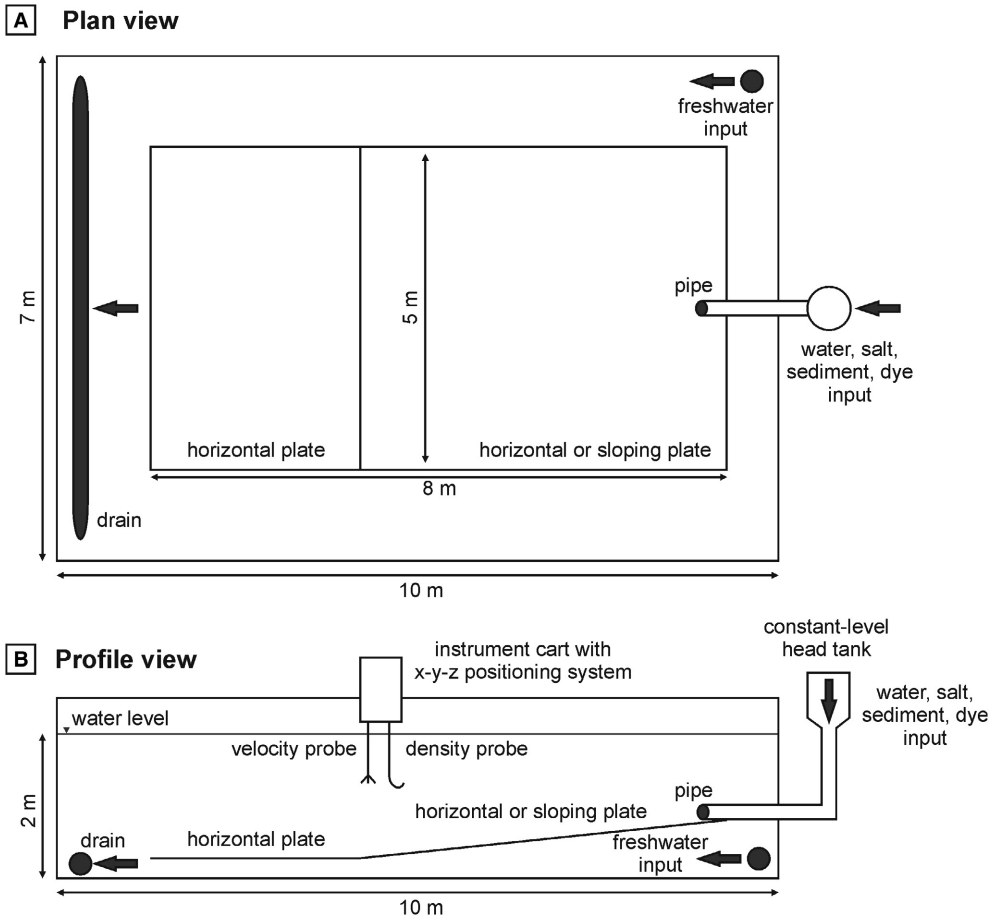

Fig. 2. Sketch of the experimental set-up. (A) Plan view. (B) Profile view.

along with sediment-transport conditions and tested with observations, using known diagrams (i.e. Shields diagram and bedform-regime diagrams). Froude scaling was checked using observed bedforms and flow conditions measured in the far-field, where flows had transitioned to gravity-dominated density flows (cf. Fedele *et al.,* 2016). The absolute value of the slope is not to be used to upscale to field conditions. Instead, due to the generally over-represented effect of friction in laboratory flows, Froude number scaling, which should be also considered as a ratio between overall friction and slope, should be used for the far-field flow, whereas a measure of the overall momentum input and gradient might be more representative of the scaling for the near-field flow conditions. However, a formal scaling between the experimental conditions and any natural system was not intended in this study, and an upscaling by a single similarity law is not possible.

To compare the behaviour of jets and density flows, two runs were conducted with density flows expanding from an inlet box. The density currents were produced by mixing water, salt and sediment into the Venturi mixing system, then pumping the brine solution and sediment to the head tank, which released the flow into the inlet box at the upstream end of the tank. The flow then left the inlet box and entered the experimental domain through the 20.5 cm wide outlet.

Data collection

The evolving jets and deposits were visually observed and documented by photographs and videos through the glass walls of the tank. After draining the tank, the deposits were documented, noting length, width, thickness and bedform wavelength. The thickness of the deposits was measured in profiles along the centreline of the flow.

Velocity and conductivity probes, along with a system of syphons for sample extraction, were used to measure detailed velocity and density profiles. Velocities were measured using a Nortek Vectrino profiler (Nortek Group, Rud, Norway), while density profiles were measured using both a calibrated conductivity probe and a system of syphons. Velocity and density time series were taken both during establishment and after deposit properties (geometry) seem to remain steady in time. Typically, time series of 1.5 min were taken at each location, allowing for the time description of the series and computation of mean values. Velocity profiles presented in this work are all time-averaged over turbulence in this time interval. Velocities were measured at a rate of 25 Hz. Both the velocity and conductivity probes and syphons were attached to a mounting tower, which was attached to an automated cart that could be controlled through a computer, allowing the positioning of the probes at any x–y–z location in the tank for collecting flow data during the experiments.

The data points of the velocity and density profiles are plotted versus the vertical elevation above the surface of the bed as it was measured by the velocity probe before, during and after the run. If sediment was present in the experiments, this is the elevation above the local bottom of the sediment surface measured. In some cases, the position of the bed could not be determined during the run due to intense bedload and suspension transport near the bed, but the position of the bed was always read before and after the measurement of the profiles. The water temperature was measured through the velocity probe before and during the runs, meaning that both the ambient and the flow temperature were measured. However, the difference was never more than 1 to 2% and the effect was therefore considered negligible.

Based on the locally measured velocity and density profiles, layer-averaged streamwise flow velocity, fractional excess density and flow thickness were computed using the Ellison–Turner-momentum equations (Ellison & Turner, 1959). The determined average values were then used to compute the densimetric Froude numbers at the locations of the measurements.

Tested flow conditions

The controlling factors on the flows and their deposits were systematically tested for their relative impact and include: (i) the initial flow density; (ii) bed erodibility; (iii) sediment discharge; (iv) bed slope; and (v) grain size (Table 1). The orifice densimetric Froude number, taken as an indicator of stratification (density), is considered a primary controlling factor and is used here also with the purpose of comparison to reported work in the literature (Rajaratnam & Berry, 1977; Hoyal *et al.,* 2003). The densimetric Froude number was controlled by adjusting both the water-flow rate and the amount of salt fed to the Venturi mixing system, by way of a pre-determined calibration curve. It is assumed here that for pure jets (non-stratified), the densimetric Froude number approaches infinity. The incoming densimetric Froude number was always well above the limit of $Fr' \geq 1.2$ that separates gravity-controlled from momentum-controlled flows (List, 1982; Powell, 1990; Roberts *et al.,* 2001). Therefore, all jets can be considered as momentum-dominated flows.

In the experiments, three different basic configurations were tested: (i) non-aggrading jets (stratified and non-stratified) on non-erodible beds; (ii) sediment-free jets (stratified and non-stratified) on erodible beds; and (iii) sediment-laden stratified jets on erodible beds. Non-aggrading conditions mean that no sediment was fed into the flow, while under aggrading conditions sediment was fed into the flow at a fixed rate. Experiments on non-erodible beds were conducted directly on a fixed bed. To provide erodible bed conditions, the fixed bed was covered by a flat sediment bed of constant thickness. The bed slope, grain size and sediment-supply rate were varied for selected configurations. To produce larger flows and deposits that are easier to measure the pipe diameter was increased during the study from 2.54 to 5.08 cm, thereby increasing the discharge from 0.16 to 0.63 l s^{-1}.

Non-aggrading jets on non-erodible beds

Experiments with non-aggrading jets on non-erodible beds (Table 1) did not involve any sediment and were conducted to observe the early jet dynamics prior to the formation of any scour or bedform. A set of pure and stratified jets were run on a horizontal, fixed bed and detailed velocity and density measurements were taken, allowing for testing and contrasting the observed hydrodynamics with well-known jet behaviour reported in the literature. In a few cases, and after the measurements were recorded, small

Table 1. Parameters of the conducted experimental runs.

			Outlet conditions				Sediment bed and supply		
Run #	Pipe diameter (cm)	Bed slope (°)	Discharge (l s^{-1})	Flow velocity (m s^{-1})	Fractional density difference $\Delta\rho/\rho$	Densimetric Froude number	Sediment bed	Sediment-supply rate (g s^{-1})	Supplied grain size
Run 1	2.54	10	0.16	0.32	0.089	2.12	~5 cm, FG	0.8	Medium
Run 2	2.54	10	0.16	0.32	0.019	4.59	~5 cm, FG	2.2	Medium
Run 3	2.54	10	0.16	0.32	0.019	4.59	~5 cm, FG	2.2	Medium
Run 4	2.54	10	0.16	0.32	0.089	2.12	~5 cm, FG	2.2	Medium
Run 5	2.54	10	0.16	0.32	0.019	4.59	None	–	–
Run 6	2.54	10	0.16	0.32	0.089	2.12	None	2.2	Medium
Run 7	2.54	10	0.16	0.32	0.019	4.59	None	–	Medium
Run 8	2.54	10	0.16	0.32	0.019	4.59	None	–	Coarse
Run 9	2.54	10	0.16	0.32	0.019	4.59	None	–	Coarse
Run 10	2.54	10	0.16	0.32	Pure jet	∞	None	–	–
Run 11	2.54	10	0.16	0.32	0.019	4.59	None	–	Fine
Run 12	2.54	10	0.16	0.32	Pure jet	∞	None	–	Fine
Run 13	2.54	10	0.16	0.32	Pure jet	∞	None	–	Medium
Run 14	2.54	10	0.16	0.32	Pure jet	∞	None	–	Coarse
Run 15	2.54	10	0.16	0.32	0.089	2.12	None	–	Coarse
Run 16	2.54	10	0.16	0.32	0.089	2.12	None	–	Fine
Run 17	2.54	0	0.16	0.32	Pure jet	∞	None	–	Fine
Run 18	2.54	0	0.16	0.32	Pure jet	∞	None	–	Coarse
Run 19	2.54	0	0.16	0.32	0.089	2.12	None	–	Fine
Run 20	2.54	0	0.16	0.32	0.089	2.12	None	–	Coarse
Run 21	2.54	0	0.16	0.32	0.019	4.59	None	–	Fine
Run 22	2.54	0	0.16	0.32	0.019	4.59	None	–	Coarse
Run 23	5.08	0	0.63	0.31	Pure jet	∞	None	–	Fine
Run 24	5.08	0	0.63	0.31	Pure jet	∞	None	–	Coarse
Run 25	5.08	0	0.63	0.31	0.049	1.99	None	–	Fine
Run 26	5.08	0	0.63	0.31	0.049	1.99	None	–	Coarse
Run 27	5.08	0	0.63	0.31	0.012	4.02	None	–	Fine
Run 28	5.08	0	0.63	0.31	0.012	4.02	None	–	Coarse
Run 29	5.08	0	0.63	0.31	0.049	1.99	~5 cm, MG	–	–
Run 30	5.08	0	0.63	0.31	0.012	4.02	~5 cm, MG	–	–
Run 31	5.08	0	0.63	0.31	Pure jet	∞	~5 cm, MG	–	–
Run 32	5.08	0	0.63	0.31	0.012	4.02	~5 cm, MG	5.4	Medium
Run 33	5.08	0	0.63	0.31	0.012	4.02	~5 cm, MG	2.2	Medium
Run 34	5.08	0	0.73	0.36	0.057	2.14	~5 cm, MG	5.4	Medium

Table 1. (continued)

			Outlet conditions				Sediment bed and supply		
Run #	Pipe diameter (cm)	Bed slope (°)	Discharge (l s^{-1})	Flow velocity (m s^{-1})	Fractional density difference $\Delta\rho/\rho$	Densimetric Froude number	Sediment bed	Sediment-supply rate (g s^{-1})	Supplied grain size
Run 35	5.08	0	0.69	0.34	0.054	2.08	~5 cm, MG	2.2	Medium
Run 36	5.08	0	0.63	0.31	Pure jet	∞	~5 cm, VCG	–	–
Run 37	5.08	0	0.63	0.31	0.012	4.02	~5 cm, VCG	–	–
Run 38	5.08	0	0.63	0.31	0.049	1.99	~5 cm, VCG	–	–
Run 39	5.08	0	0.63	0.31	0.012	4.02	~5 cm, VCG	2.7	Very coarse
Run 40	5.08	0	0.63	0.31	0.049	1.99	~5 cm, VCG	2.7	Very coarse
Run 41	5.08	0	0.63	0.31	0.049	1.99	~5 cm, VCG	6.4	Very coarse
Run 42	5.08	0	0.63	0.31	0.012	4.02	~5 cm, VCG	6.4	Very coarse
Run 43	5.08	10	0.63	0.31	0.049	1.99	~5 cm, FG	6.4	Very coarse
Run 44	5.08	10	0.63	0.31	0.012	4.02	~5 cm, FG	6.4	Very coarse
Run 45	5.08	10	0.63	0.31	0.027	2.68	~5 cm, FG	6.4	Very coarse
Run 46	5.08	10	0.63	0.31	0.049	1.99	~5 cm, FG	6.5	Mixed fine & very coarse
Run 47	5.08	10	0.63	0.31	0.049	1.99	~5 cm, FG	8.7	Fine
Run 48	5.08	10	0.63	0.31	0.049	1.99	~5 cm, FG	8.7	Fine
Run 49	5.08	10	0.63	0.31	0.012	4.02	~5 cm, FG	8.7	Fine
Run 50	Inlet box	10	0.63	1.06	0.050	?	~5 cm, FG	8.7	Fine
Run 51	Inlet box	10	0.63	1.06	0.050	?	~5 cm, FG	10.4	Very coarse

Abbreviations in the Sediment bed column: FG, fine-grained; MG, medium-grained; VCG, very coarse-grained.

amounts of sediment (*ca* 1 to 3 l) were fed into the flow to observe the initial formation of bedforms. Different grain sizes were used to test the effect of the sediment grain size on these bedforms.

Non-aggrading jets on erodible beds

Experiments with non-aggrading jets on erodible beds were conducted on a *ca* 5 cm thick flat sediment bed (Table 1). The configuration allowed for the observation of sediment entrainment and re-deposition by the jets and the impact of the scour and mouth-bar evolution on flow dynamics. Measurements of the flow velocity and density were recorded during some of the runs. To observe the effect of different grain sizes, sediment beds consisting of medium-grained and very coarse-grained sediment were tested.

Aggrading jets on erodible beds

Experiments with aggrading jets (i.e. sediment fed to the flow through the Venturi mixing system) on erodible beds were conducted on *ca* 5 cm thick, initially flat sediment beds (Table 1). This configuration allowed for observations and measurements of the more complex morphodynamic evolution, basic hydrodynamics and sediment-transport processes all together. Sediment was fed into the flow at constant rates. Different feeding rates were used to test the effect of sediment discharge in the flow. To observe the role of different grain sizes fine-grained, medium-grained, coarse-grained and very-coarse grained sediment was used for the bed and the sediment supply. Some runs were conducted with sediment mixed with similarly sized crushed walnut shells to highlight the internal structure of the deposit.

Density flows

Experiments with density flows released from an inlet box were conducted on *ca* 5 cm thick inclined (10°) fine-grained sediment beds (Table 1). The discharge, initial flow density and sediment supply were set to match the conditions in selected jet experiments. Different grain sizes were supplied to test the effect of the grain size as well.

RESULTS

Jets

The wall jets expanded freely from the orifice, running over the plate (with or without initial sediment bed) producing turbulent mixing at the flow interfaces (Fig. 1A to D). Hydraulic jumps were neither observed in the expanding jets nor at the transition into density flows. Flow measurements were used to support these observations. Sedimentary features and successions observed in the experiments included early-stage bedforms, scours and mouth bars, and bedforms related to the density flows beyond the scour and mouth bar (Fig. 1E).

The transition from jet to density flow was observed to occur at a short distance from the orifice, approximately at the mouth-bar crest. The decelerated flow, with negligible jet momentum remaining, was pushed over the mouth-bar crest by the incoming flow, promoting the formation of a density flow down the lee-side of the mouth bar and beyond, aided naturally by the mouth-bar lee topographic gradient. In experiments with sloping beds, the jet momentum-dominated region propagated farther downstream, but transition to density flows was more abrupt and density flows formed very fast. In most cases, density flows led to the formation of bedforms downflow of the mouth bar. In experiments with pure jets, the characteristic growth of the mixing zone was observed and measured. In addition, and when observable from the velocity profile measurements, the boundary layer growth, controlled by friction and flow expansion, was also detected (Fig. 3A to D).

Flow dynamics

Profiles of the flow velocity and density were measured at different locations along the centreline of the flow and resulting scour and mouth bar. The measured data show different hydrodynamic behaviour between: (i) sediment-free settings and settings with sediment; and (ii) pure jets (non-stratified) and stratified dense jets. Experiments with expanding (3D) pure wall-jets on non-erodible horizontal beds provided a baseline for testing and for verification and comparison with reported results (cf. Wu & Rajaratnam, 1995; Craft & Launder, 2001). Observations and results from the measurements for the present study agree well with the known basic hydraulics of these flows. A comparison of the downstream changes in flow thickness for selected runs, including pure jets over fixed or erodible beds, is shown in Fig. 3E. Dimensionless scaling of the distance and flow thickness was used to maintain consistency, and for comparison purposes with reported experimental data. The dimensionless length scale x/D_0, where x is the distance from the orifice and D_0 is the orifice diameter, is plotted against the dimensionless flow-thickness scale B/D_0, where B is the height of the half of the peak velocity above the bed. The data for 3D pure jets display a straight rising trend due to downflow thickening of the flow (Fig. 3E). The thickening trend of the pure 3D jets has a much lower rate when compared to the trends known from previous studies of 2D jets (Rajaratnam & Subramanyam, 1986). Previous studies by Launder & Rodi (1983) have shown that the lateral spreading always exceeds the vertical spreading, thereby reducing the thickening of the flow. The thickness increase rate for 3D pure wall jets obtained from the measurements herein agrees with reported values obtained experimentally and numerically (e.g. Craft & Launder, 2001). Dense jets display even smaller rates of flow-thickness increase, presumably because of flow stratification (Fig. 3E).

Non-aggrading jets on non-erodible (fixed) horizontal beds (sediment-free setting) are characterized by a velocity peak close to the bed (Fig. 3A to C). This velocity peak indicates the top of the boundary-layer flow controlled by bed friction. Above the velocity maximum, velocities display the typical upward decrease (with upward turbulent diffusion) to the ambient water body. The downflow deceleration with distance from the orifice is shown in Fig. 3F. The dimensionless length scale x/D_0, where x is the distance from the orifice and D_0 is the orifice diameter, is plotted against the dimensionless flow-velocity scale u/u_0, where u is the peak velocity at a given location and u_o is the velocity at the orifice. Pure jets and low-density stratified

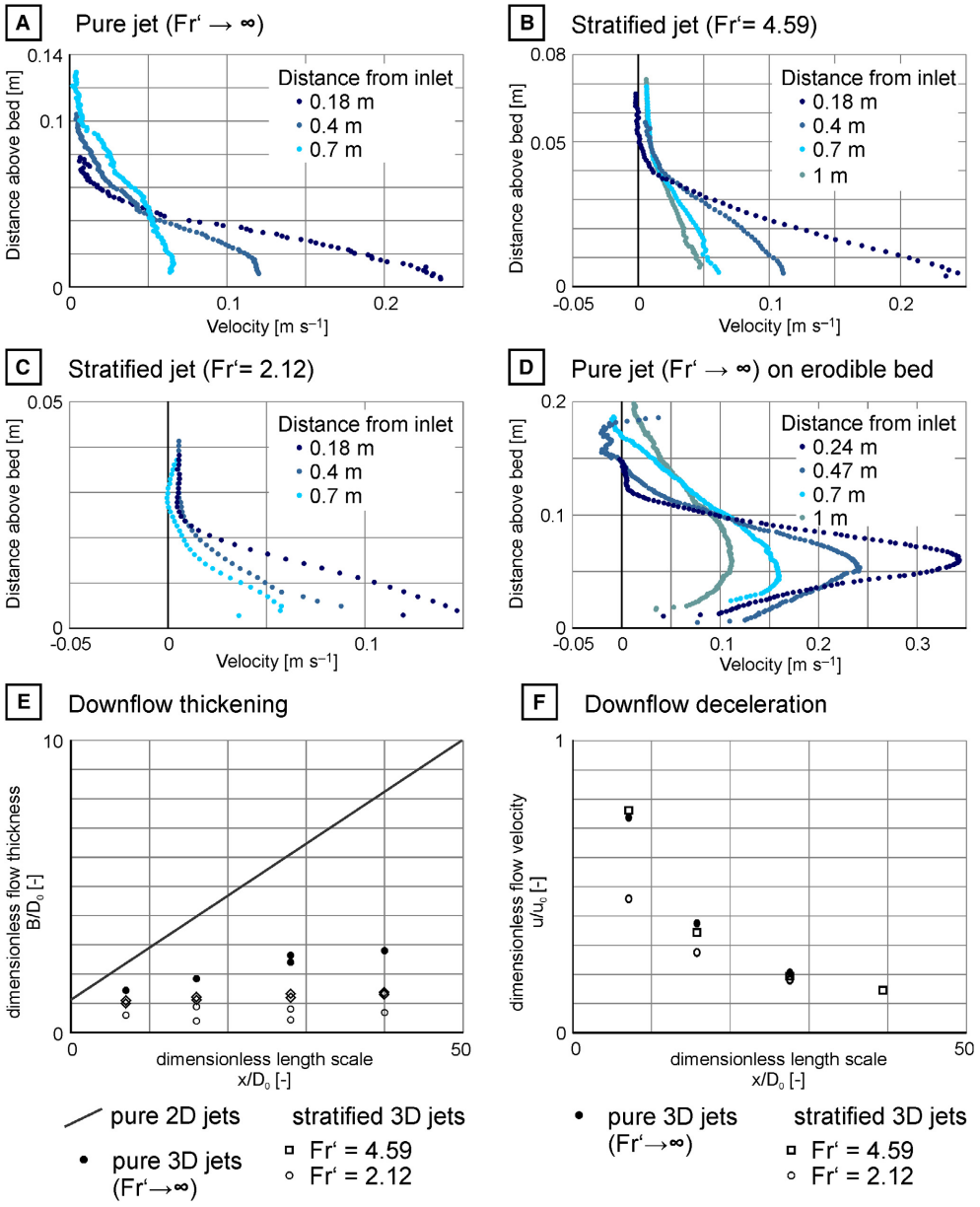

Fig. 3. (A) to (D) Velocity profiles of jets measured at different distances from the inlet. The distance above the bed is measured from the surface of the (sediment) bed. Note the different scales used for the plots. (A) Non-aggrading jet (Fr' → ∞) on non-erodible bed (run 17). (B) Non-aggrading stratified jet (Fr′ = 2.12) on non-erodible bed (run 21). (C) Non-aggrading stratified jet (Fr′ = 4.59) on non-erodible bed (run 19). (D) Non-aggrading jet (Fr' → ∞) on erodible bed (run 31). The data points have been corrected for the elevation above the sediment bed at the end of the run. (E) Downflow thickening of jets. The fit line for pure 2D jets is from Rajaratnam & Subramanyam (1986). x/D_0 is a dimensionless length scale, where x is the distance from the orifice and D_0 is the orifice diameter. B/D_0 is the dimensionless flow thickness, where 'B' is the height of the half of the peak velocity above the bed. (F) Downflow deceleration of jets. The dimensionless length scale x/D_0, where x is the distance from the orifice and D_0 is the orifice diameter, is plotted against the dimensionless flow-velocity scale u/u_0, where u is the peak velocity at a given location and u_0 is the velocity at the orifice.

jets display an almost indistinguishable behaviour, while high-density stratified jets display a more pronounced deceleration closer to the orifice (Fig. 3F). The density difference in high-density jets aids not only on the transition to gravity-dominated density flows in the far-field,

but also appears to decrease mixing in the momentum-dominated near-field. In stratified wall jets the rate of increase in flow thickness in downflow direction is smaller when compared to pure (non-stratified) wall jets (Fig. 3A to C). The elevation of the velocity peak above the bed tends to decrease and then slowly increase in the far-field distal region, presumably responding to first flow expansion and then increasing effects of density difference and bed friction. In the uppermost sections of the time-averaged profiles, velocities show on occasion small excursions, including negative values, suggesting small counterflows and/or the dominant effects of turbulent fluctuations over weaker mean flow. Due to the very low elevation of the velocity peak the lower boundary layer of sediment-free jets was poorly resolved by the velocity measurements (Fig. 3A to C).

In experiments with non-aggrading jets on erodible beds the measurements were conducted when the growth of the scour and mouth bar had ceased (i.e. approximate dynamic equilibrium). Measurements from experiments with sediment beds indicate strong interaction and feedback of the flow with the bed and developing bedforms. Velocity measurements very close to the bed are partly affected by the presence of high concentrations of sediment in the flow, causing a low 'signal to noise' ratio or loss of the signal from the probe. The downflow evolution of the velocity profiles varies between different experimental settings and conditions (Figs 3D, 4 and 5), reflecting the rich variety of flow processes and complex flow configurations taking place. Measurements from a pure wall jet display an almost symmetrical velocity profile near the orifice with a very pronounced velocity peak, resembling an axisymmetrical jet (Figs 3D and 4B). With increasing distance to the orifice, the maximum velocity decreases and moves closer to the bed, presumably due to flow expansion or an increase in flow density by sediment entrainment. The development of the scour reflects the dissipation of initial momentum when an erodible bed is present. The maximum depth of the scour is a function of incoming momentum in the jet, density of the incoming fluid, and sediment properties.

The flow configuration in the scour at equilibrium is complex. The core of the dense jet tends to plunge into the deepest part of scour, deepening the scour as the density of the incoming flow increases. A reversed flow cell moves towards the steeper upflow slope of the scour, while most of the jet continues downflow and moves along the less steep downflow slope of the scour and over the mouth-bar crest (Fig. 4A). A boundary layer associated with this portion of the flow develops as it moves towards the crest, with a secondary recirculation and reversed flow, depending on their relative densities (Figs 4 and 5). While this secondary recirculation over the developing boundary layer might resemble an internal hydraulic jump, it is probably a more fundamental hydrodynamic behaviour, characteristic of the near flow field and spreading of momentum-driven wall jets. As the flow begins to expand, streamwise gradients of both vertical and lateral components of the velocity are positive, producing vorticity sources opposite to those in the fully developed, far-field flow, and thus promoting the characteristic velocity distribution with recirculation (cf. Launder & Rodi, 1983). The recirculation may be enhanced by the curvature of the scour and the adverse topographic slope, which the developing boundary layer encounters as the flow expands and moves towards the mouth-bar crest. The measurements here suggest that the recirculation is dependent on the overall internal flow structure and variation of the density field in the scour. Visual observations and measurements suggest that the boundary layer moving along the scour bed remains thin and does not thicken as it moves towards the mouth-bar crest, indicating the absence of the characteristic flow thickening associated with hydraulic regime change through a hydraulic jump.

Farther downflow and beyond the crest of the mouth bar, velocity profiles show the classic patterns of gravity-dominated density flows, with a pronounced velocity peak in the lower part of the flow, and velocity decay upward (Figs 4 and 5). While wall jets in the near-field might present similar patterns, it is important to note that most measurements show an increase in the peak velocity as the flow moves from the crest and away downstream on the lee side of the mouth bar, indicating flow acceleration induced by the mouth-bar slope and the density difference (Figs 4C and 5A). The acceleration is higher in denser flows even if mouth-bar slopes are lower, thus supporting the argument of a classic gravity-dominated density flow.

Density profiles measured for the stratified jets generally show a general decrease of the flow density with increasing distance from the orifice (Figs 4C, 5 and 6). The density profiles also show various trends including increasing

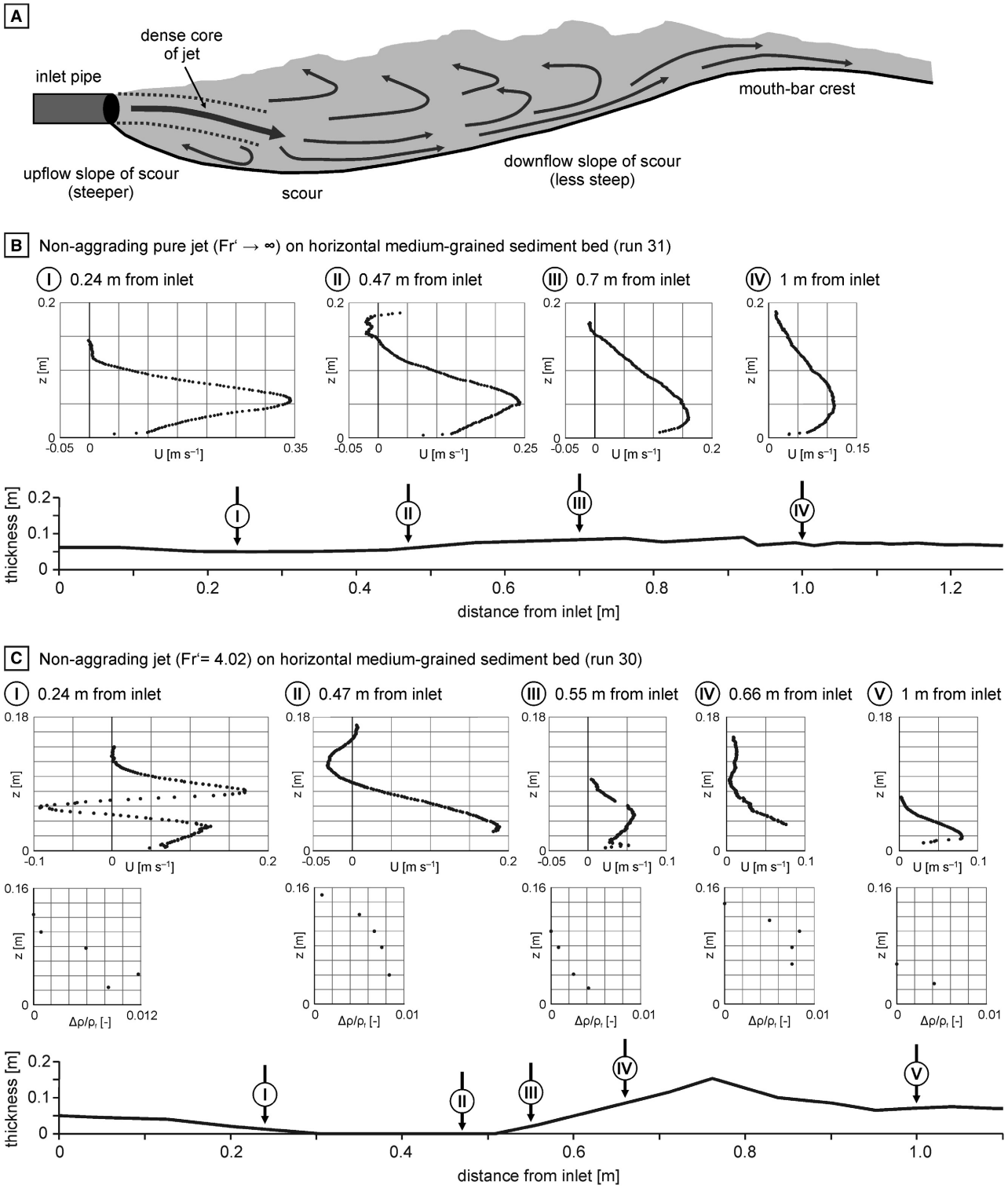

Fig. 4. Downflow evolution of jets on horizontal erodible beds. (A) Schematic sketch to illustrate the complex flow evolution with the scour, based on visual observations and measurements. (B) and (C) Plots of the profiles of the velocity (U) and the fractional density difference ($\Delta\rho/\rho_f$) above the surface of the sediment bed (z). The locations of the measurements are indicated above thickness profiles of the sediment beds. (B) Non-aggrading pure jet ($Fr' \rightarrow \infty$). (C) Non-aggrading stratified jet ($Fr' = 4.02$).

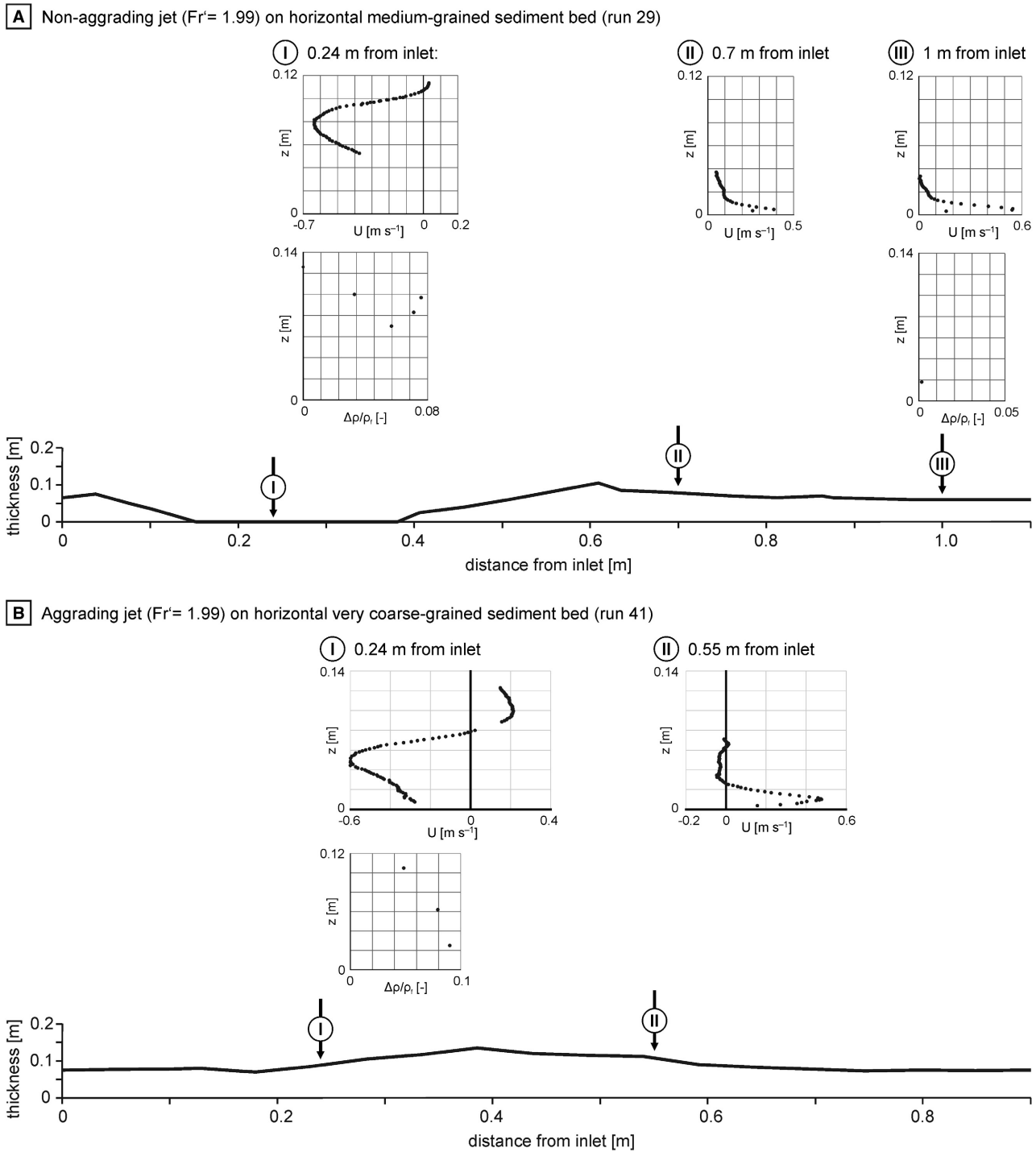

Fig. 5. Downflow evolution of jets on horizontal erodible beds. Plots show the profiles of the velocity (U) and the fractional density difference ($\Delta\rho/\rho_f$) above the surface of the sediment bed (z). The locations of the measurements are indicated above thickness profiles of the sediment beds. (A) Non-aggrading stratified jet ($Fr' = 1.99$). (B) Aggrading stratified jet ($Fr' = 1.99$) with a sediment-supply rate of 6.4 g s^{-1}.

upward profiles with or without inflexion points (with highest density values near the bed), and in some cases with unstable stratification (for example, increasing and then decreasing density with distance from the bed; Figs 4C, 5 and 6). Denser fluid flowing up in the core of the flow

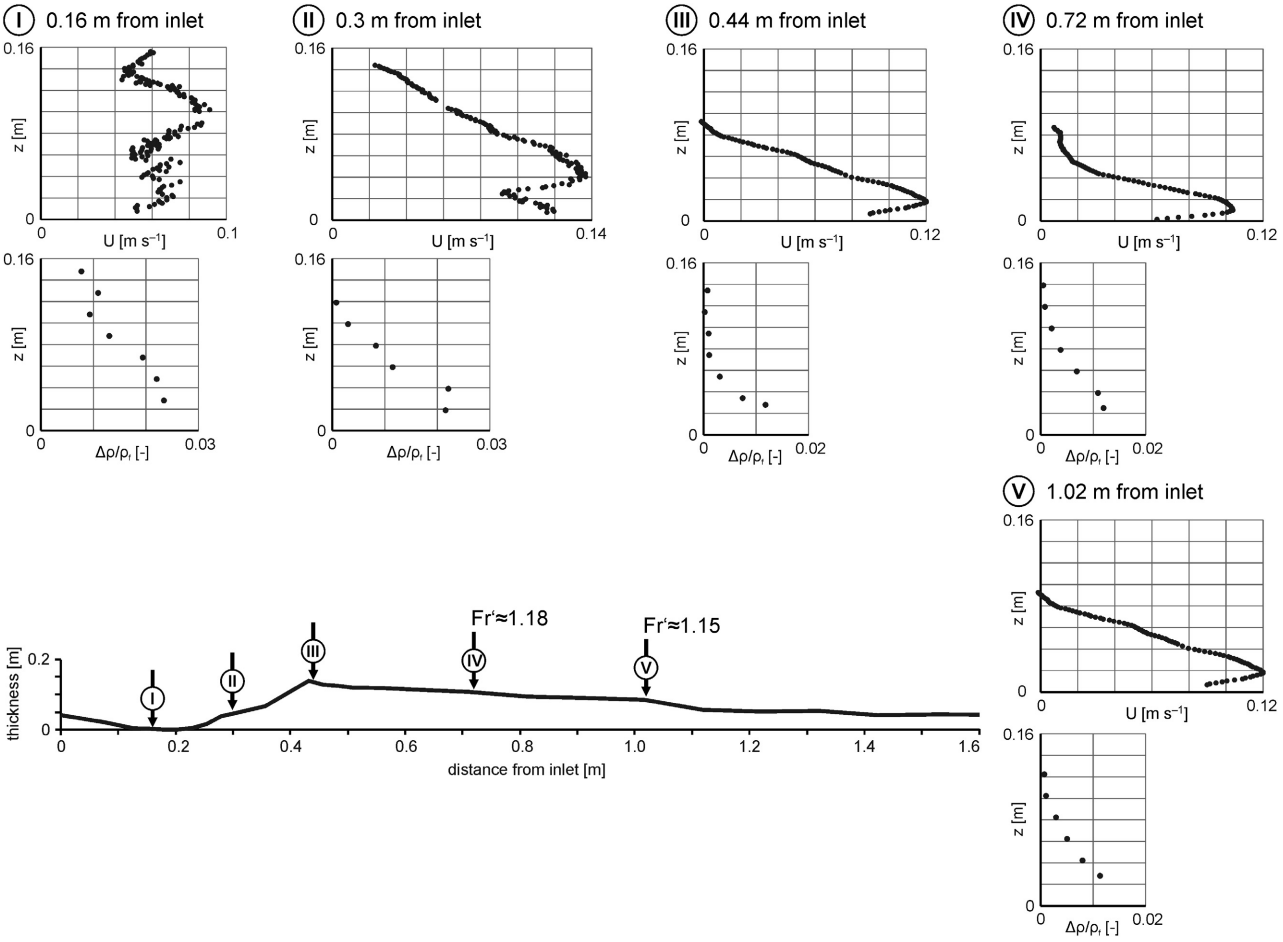

Fig. 6. Downflow evolution of a jet on an inclined (10°) fine-grained sediment bed (Fr′ = 2; sediment-supply rate 6.4 g s^{-1}; very coarse-grained sediment, run 43). Plots show the profiles of the velocity (U) and profiles of the fractional density difference ($\Delta\rho/\rho_f$) above the surface of the sediment bed (z). The locations of the measurements are indicated above the thickness profile of the sediment bed.

within the scour might be associated with the complex flow recirculation established in those regions. The relations between velocity and density profiles measured at different locations are in general complex, and highly variable, suggesting complex phenomena that deserve further detailed investigation.

Erosion and deposition

The erosion of scours and the deposition of mouth bars and bedforms were observed in all experiments involving sediment. Sediment fed into the jet was transported as both bedload and suspended load. Bedload sheets dominated the sediment transport at the orifice and near-field region, during both early and final steady stages in the deposit morphology evolution. Small-scale turbulent bursts were observed to impact the inner margins of the scour and mouth bar, clearly derived from transformation and dissipation of the initial momentum of the jet. These impacts entrained sediment and triggered grain avalanches, which allowed for the entrainment of more sediment. The entrained sediment was either deposited on the inner mouth-bar margin or transported over the mouth-bar crest, and these processes continued even during the final, more steady state configuration of the deposit, in dynamic equilibrium. Downflow of the mouth-bar crest deposition and erosion were generally, and clearly, associated with the density flow.

Early-stage bedforms

Concentric bedforms formed during the early stages of deposit evolution and commonly preceded the formation of the scour and mouth bar (Fig. 7). Their formation was very rapid and

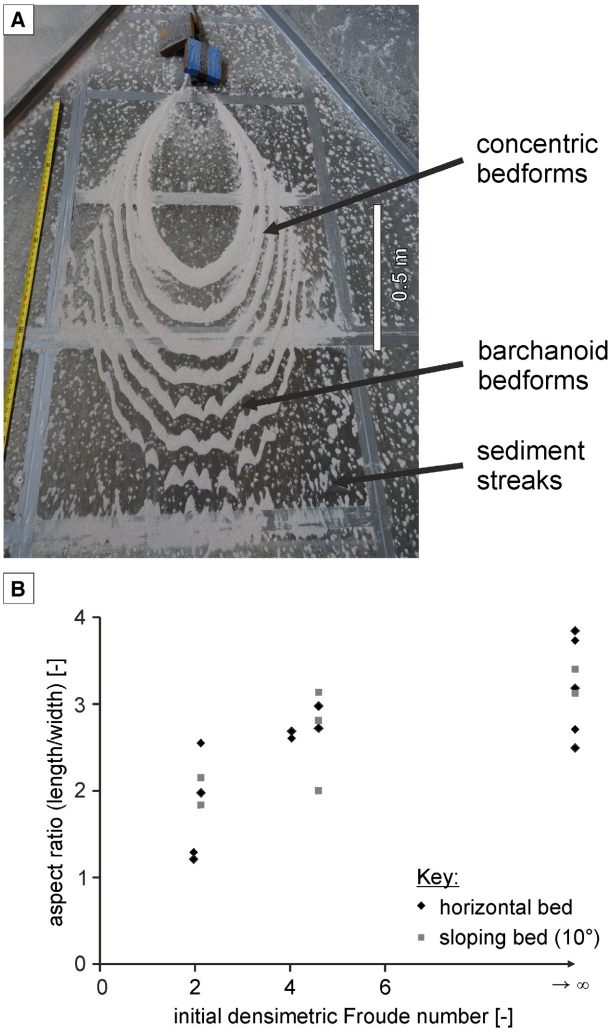

Fig. 7. Deposition by non-aggrading jets on non-erodible beds after a small amount of sediment was fed into the flow. (A) Example of early-stage bedforms (plan view). Concentric bedforms pass downflow into discontinuous barchanoid bedforms and thin sediment streaks ($Fr' = 2.12$; bed slope $S = 10°$; fine-grained sediment; run 16). (B) Plots of the initial densimetric Froude number against the aspect ratio (crestal length/width) of the mouth bar for jets on horizontal and sloping beds.

occurred within a few minutes after the start of the flow or sediment feed, respectively. Interestingly, the best observations of these precursor bedforms were possible in experiments with non-aggrading jets on non-erodible beds, when only small quantities of sediment were supplied, immediately imprinting patterns of deposition on the fixed bed, thus suggesting a strong flow control. On horizontal beds the concentric bedforms became stationary in both geometric properties and position (i.e. without migration) at a certain distance from the inlet.

In most experiments, the early-stage concentric bedforms displayed asymmetrical geometries with gentle stoss sides and steep lee sides (Fig. 7A). Bedform wavelengths ranged from 6 to 12 cm and heights from 0.5 to 2.0 cm, with downflow decreasing bedform heights. The total number of these concentric bedforms at equilibrium ranged from two to eight and was controlled by the bed slope, initial density difference, grain size and the amount of sediment fed into the flow at the inlet. Experiments on sloping beds produced more concentric bedforms along with a wider variety of isolated bedforms than those on horizontal beds.

The aspect ratio (length versus width) of the bedform crests increased with increasing densimetric Froude number, displaying logarithmic-style trends (Figs 7B and 8A). At lower densimetric Froude numbers, the bedforms displayed plan view geometries with low elongation and a high degree of lateral spreading. At higher densimetric Froude numbers, the plan-view geometry of the bedforms became more elongated (Fig. 7B). Typically, the proximal bedforms were concentric with continuous crests, while the distal bedforms were more isolated with barchanoid or rhomboid shapes. The most distal bedforms were thin longitudinal streaks parallel to the flow direction (Fig. 7A).

Early-stage bedforms are interpreted as representing small-scale dunes. This interpretation is based on their asymmetrical geometry, the visually observed interactions of the bedforms and the flows aided by dye injection, the measured flow velocities, and scaling estimates between bedform wavelength and flow thickness. The early-stage bedforms showed complex interaction patterns with the flow, none of which showed in-phase (antidune-like) flow-bed relation. Sediment was deposited on their lee sides by small-scale eddies. Changes in bedform geometry and lateral continuity are related to downflow velocity decay and/or sediment starvation in non-aggrading flows. Further away from the near-field region, asymmetrical bedforms also formed but these were interpreted as ripples, because they formed in regions of slower, and thus weaker, flow and the wavelength scaling responded more to grain size.

Scour and mouth bar

Scours and mouth bars formed in all experiments with erodible beds regardless of the

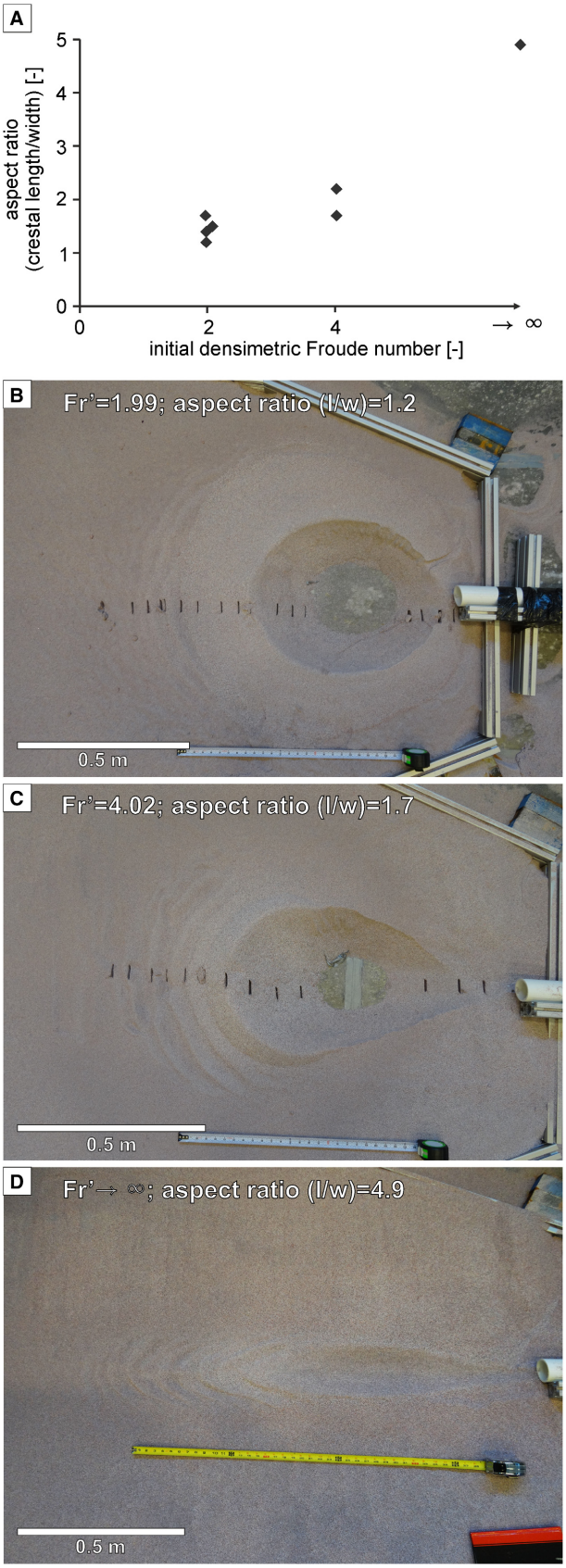

Fig. 8. Characteristics of the mouth bars deposited by the experimental jets. (A) Initial densimetric Froude number plotted against the aspect ratio (crestal length/width) of the mouth bar. (B), (C) and (D) Photographs of mouth bars deposited by non-aggrading jets on horizontal, medium-grained sediment beds. (B) Initial densimetric Froude number Fr′ = 1.99. (C) Initial densimetric Froude number Fr′ = 4.02. (D) Initial densimetric Froude number Fr′ → ∞.

sediment supply (Figs 8 and 9), presumably as a result of the strong influx of momentum by the jet in the near-field. The scour margins always connected to the orifice and were surrounded by a mouth bar (Fig. 8B, C and D). The geometry and dimensions of the scour and mouth bar were controlled by the initial density difference, grain size, sediment supply and bed slope. The scour aspect ratio (length versus width) increased with the value of the efflux densimetric Froude number (Fig. 8A). The dimensions of the scour and mouth bar showed an overall negative correlation with the grain size, i.e. both length and width of the scour and mouth bar decreased with increasing grain size. All other remaining parameters seemed to have much less control on the scour and mouth-bar geometric properties. The mouth-bar height increased at higher sediment supply and decreased on inclined beds.

The scour depth was strongly controlled by the initial density of the influx. The scour depth increased for denser efflux (lower initial densimetric Froude numbers), reflecting a strong control of gravity over the initial momentum of the jet (Fig. 9A to C). In some experiments, the true depth of the scour could not be measured because the sediment was completely removed from the plate (original thickness *ca* 5 cm). At the lowest densimetric Froude numbers tested (Fr′ = 2) the scoured area became largest and, at constant sediment supply, the scour remained deeper also for lower Froude numbers (Fig. 9B and C). The inner side walls of the scours were very steep and at the angle of repose or slightly steeper, as indicated by the slope failures during the later dynamic-equilibrium stages. The slope failures in the scour inner walls were observed to occur frequently, transporting sediment towards the centre of the scour. There, the sediment was partly entrained by eddies from the jet and either re-deposited on the mouth bar or bypassed. The size of the scour was also affected

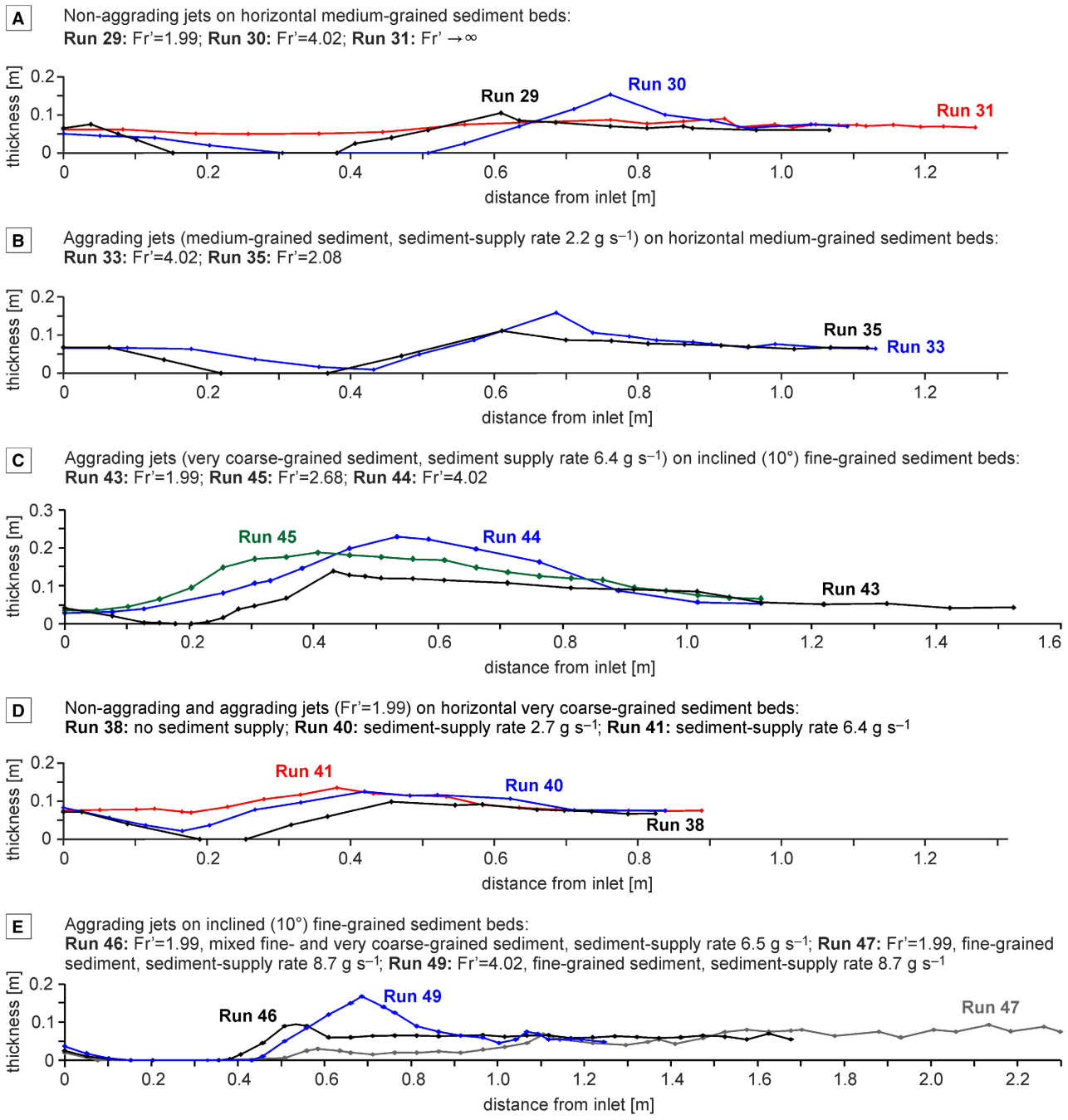

Fig. 9. Thickness profiles of the jet deposits. Note the different horizontal scales. (A) Thickness profiles of non-aggrading jet deposits on horizontal, medium-grained sediment beds at different initial densimetric Froude numbers. (B) Thickness profiles of aggrading jet deposits on horizontal medium-grained sediment beds at constant sediment-supply rates (2.2 g s^{-1}) of medium-grained sediment and different initial densimetric Froude numbers. (C) Thickness profiles of aggrading jet deposits on inclined (10°) fine-grained sediment beds at different initial densimetric Froude numbers and a supply of very coarse-grained sediment at constant sediment-supply rates (6.4 g s^{-1}). (D) Thickness profiles of aggrading jet deposits on horizontal very coarse-grained sediment beds at constant initial densimetric Froude numbers (Fr′ = 1.99) and a supply of very coarse-grained sediment at different sediment-supply rates. (E) Thickness profiles of aggrading jet deposits on inclined (10°) fine-grained sediment beds at different initial densimetric Froude numbers and different grain-sizes and supply rates of the sediment.

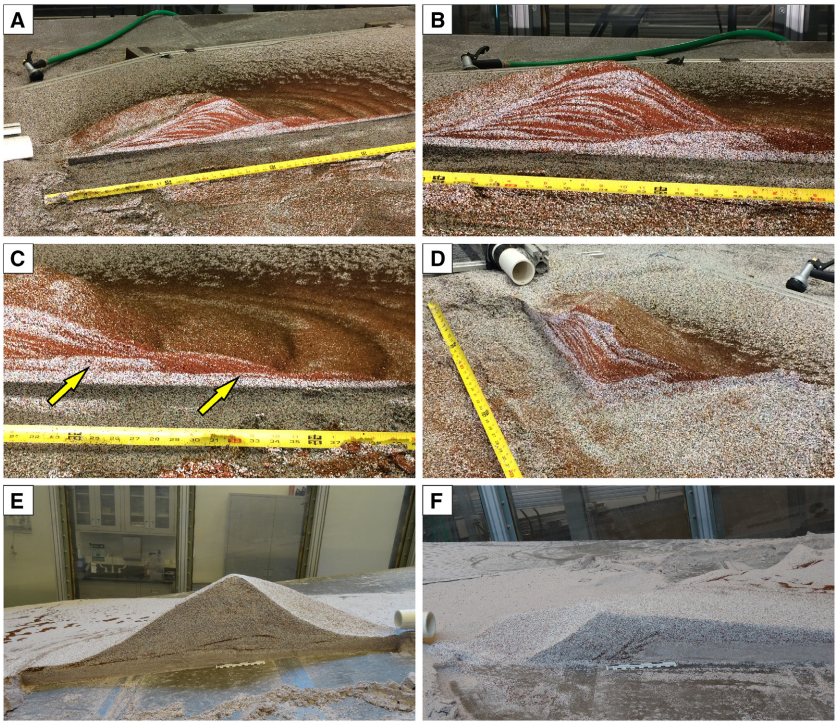

Fig. 10. Internal mouth-bar architecture. (A) to (D) Internal architecture of a mouth bar deposited on a very coarse-grained horizontal sediment bed ($Fr' = 4.02$; very coarse-grained sediment, sediment-supply rate 6.4 g s^{-1}, run 42). (A) and (B) Asymmetrical downflow divergent convex-up stratification in a section parallel to the flow direction. (C) Progradation of the mouth-bar deposits above the early-stage bedforms (arrows). (D) Section perpendicular to the flow direction, displaying concentric convex-up stratification. (E) Internal architecture of a mouth bar deposited on a fine-grained inclined (10°) sediment bed ($Fr' = 4.02$; very coarse-grained sediment; sediment-supply rate 6.4 g s^{-1}, run 44). The shallow scour at the base is infilled and overlain by the convex-up stratification of the growing mouth bar. (F) Internal architecture of a mouth bar deposited on a fine-grained inclined (10°) sediment bed ($Fr' = 1.99$; very coarse-grained sediment; sediment-supply rate 6.4 g s^{-1}, run 43). The upflow-dipping strata of the mouth bar infill the scour and resemble backset cross-stratification.

by the grain size of the sediment bed, for the cases in which sediment supplied in the flow was of a different size than that forming the initial bed. Finer-grained sediment beds resulted in larger and deeper scours and vice versa.

Aggrading jets led to the vertical and lateral mouth-bar growth and infilling of the scour. If the sediment supply was increased, infilling of the scour by bedload sheets shed from the orifice was more significant than the growth of the mouth bar, reducing the height difference between the scour base and the mouth-bar crest (Fig. 9D).

Sediment movement on the lee sides of the mouth bar was related to sustained density flows and grain avalanches. Small-scale bedforms were commonly observed on the frontal distal side of the mouth bar, displaying concentric crests, and emanating from the crest of the mouth bar, reflecting the dense flow direction (Fig. 8B to D). In most experiments two to four rounded and symmetrical bedforms occurred. These bedforms had wavelengths of 4 to 7 cm and heights of 0.2 to 0.5 cm. The rounded bedforms appeared to be in-phase with the overriding density flow, typically in the near frontal part of the mouth bar, and appear to be stationary but in a few cases they migrated downstream. These features were interpreted as antidunes, because they were mostly formed where topographic gradient of the mouth bar induced stronger density flows. Grain avalanches derived from slope failures accounted for the localized re-mobilization of sediment deposited on the lateral lee sides of the mouth bar.

Internal mouth-bar architecture

The internal architecture of the jet-flow deposits (scour and mouth bar) could be observed only

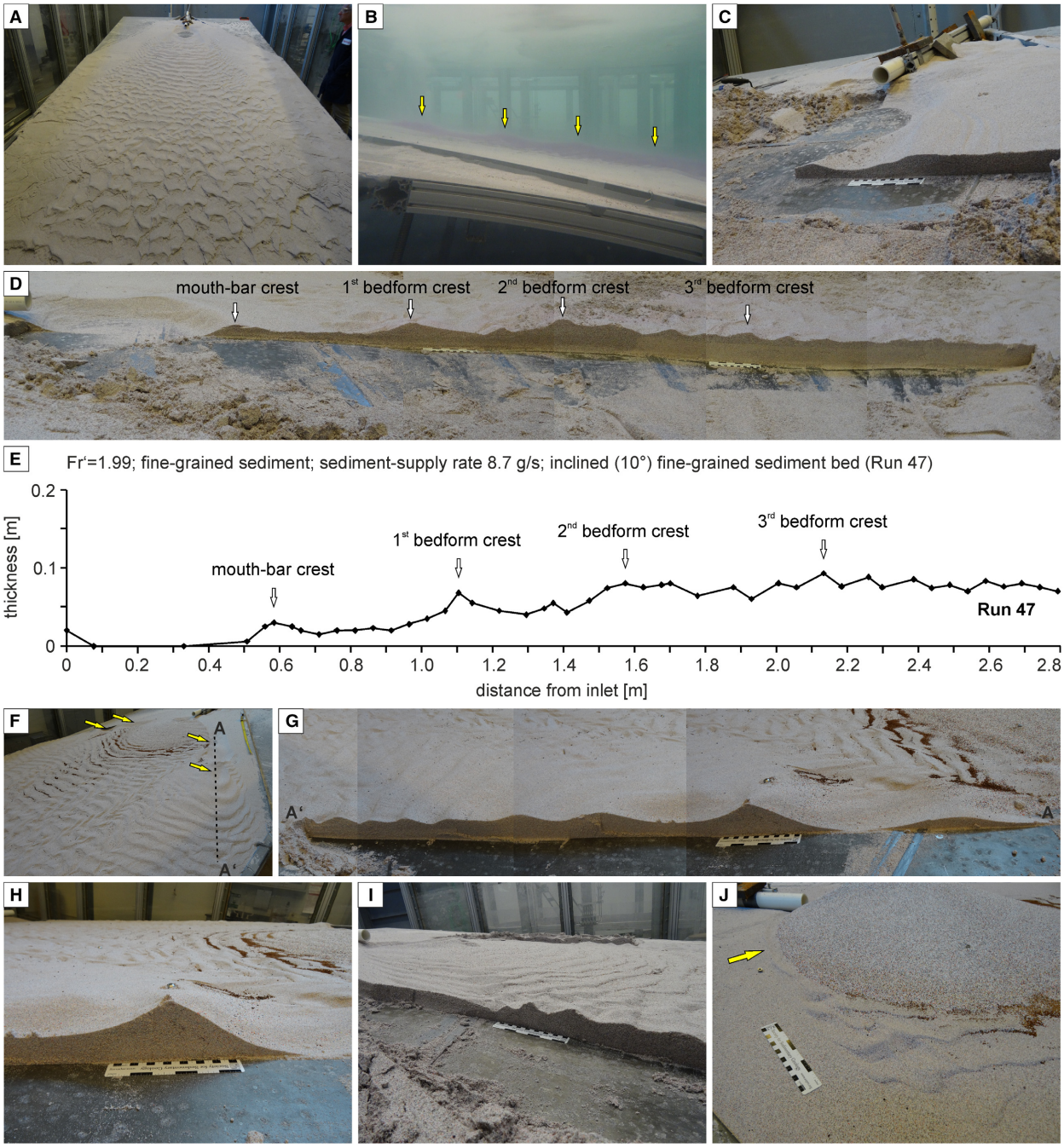

Fig. 11. Bedforms deposited by density flows downflow of the jet-mouth bar. (A) Oblique view of the bedforms (Fr′ = 1.99; bed slope 10°; fine-grained sediment; sediment-supply rate 8.7 g s^{-1}; run 48). (B) Formation of a train of in-phase waves during run 47. (C) Flow normal cross-section, showing a secondary scour laterally adjacent to the jet-scour and mouth bar (Fr′ = 1.99; bed slope 10°; fine-grained sediment; sediment-supply rate 8.7 g s^{-1}; run 48). (D) Photographic panel (mirrored to match the orientation of the measured profile) and (E) thickness profile of the in-phase bedforms deposited during run 47. (F), (G) and (H) Formation of bedforms laterally adjacent to the mouth bar (Fr′ = 1.99; bed slope 10°, very coarse-grained sediment; sediment-supply rate 6.4 g s^{-1}; run 43). Arrows indicate deep scours at the upflow end of bedform trains. (F) Oblique view of the bedforms. (G) Cross-section of the bedforms (A–A‘ in Fig. 11F). (H) Detail of the first asymmetrical bedform, showing upflow dipping cross-lamination. (I) Train of bedforms developed laterally adjacent to the mouth bar (Fr′ = 1.99; bed slope 10°, mix of fine-grained and very coarse-grained sediment; sediment-supply rate 6.5 g s^{-1}; run 46). (J) Formation of a small channel-like feature (arrow) due to flow splitting around the mouth bar (Fr′ = 2.68; bed slope 10°, very coarse-grained sediment; sediment-supply rate 6.4 g s^{-1}; run 45).

in few runs, for which crushed walnut shells were supplied in small pulses with the purpose of visualizing the internal bedding, and posterior dissection of the deposits was performed. Internally, mouth bars are characterized by asymmetrical downflow divergent convex-up stratification (Fig. 10), producing distinct upflow-dipping ('mouth-bar topset') and downflow-dipping ('mouth-bar foreset') strata. The core of the mouth bar is formed by a symmetrical mound. Upflow-dipping strata dip gently (*ca* 15°) and thin and steepen upward. Downflow-dipping strata dip steeply (*ca* 30°) and thicken and steepen upward. In sections perpendicular to the flow, mouth bars are characterized by symmetrical convex-up stratification (Fig. 10D). Scouring of the bed precedes mouth-bar deposition. Scours are backfilled when deposition exceeds erosion (Figs 9D, 10E and 10F). The infill of the deeper scours with the upflow-dipping strata of the mouth bar resembles backset cross-stratification known from hydraulic-jump zones (Fig. 10F). Overall, the internal architecture of the mouth bars matches their strong progradation observed during the experiments, particularly before reaching dynamic equilibrium. The mouth-bar deposits prograded over the early-stage bedforms (Fig. 10B and C) as they were growing in height and overall size.

Bedforms beyond the mouth bar

In runs with inclined beds bedforms were widespread over the plate (Fig. 11). The formation of these bedforms was related to the density flow and commenced within the first few minutes after the start of the flow. During the experiments, different bedform fields evolved downflow and laterally adjacent to the mouth bar. Two different trends were observed, depending on the supplied grain sizes. The supply of fine-grained sediment triggered the formation of bedform trains immediately downflow of a low mouth bar (i.e. in the centreline of the initial jet), while the supply of coarse-grained sediment triggered the formation of symmetrical lateral bedform trains on both sides of a high mouth bar.

Bedform fields downflow of the mouth bar were prominent in runs where fine-grained sediment was supplied and mouth-bar aggradation remained low (Fig. 9E and F). Under these conditions the density flow largely followed the centreline of the jet flow and trains of bedforms evolved (Fig. 11B to E). Observations aided by dye in the flow during the runs showed clear in-phase relation between the bedforms and the upper interface of the density flow (Fig. 11B). In these runs the thickness of the mouth bars was lower than the thickness of the original sediment bed. The change from degradation to aggradation of the bed occurred 1.2 to 1.4 m from the inlet (Fig. 11E). In general, a first couple of larger bedforms were observed with clear symmetrical shape, while asymmetrical, smaller bedforms with a steeper lee side prevailed beyond. In plan-view the large bedforms displayed fairly straight crests, appeared stationary, and showed wavelengths that ranged from 41 to 56 cm (mean: 48.5 cm) and thicknesses that ranged from 5.5 to 9.3 cm, but increased downflow (Fig. 11D and E). Superimposed smaller scale bedforms had wavelengths of *ca* 10 cm, heights of 1 to 3 cm and were asymmetrical with steeper lee sides (Fig. 11D and E).

Bedform fields laterally adjacent to the mouth bar were prominent in runs where coarse-grained sediment was supplied and mouth-bar aggradation was high (Figs 9E and 11F to J). Under these conditions flow splitting around the mouth bar occurred, diverting some flow from the scour to the lateral sides in the form of stronger gravity-dominated density flows. These laterally diverted flows first tended to spread and expand, but later bedform trains suggest flow convergence. Increased bedload transport between flows going around and from the lateral sides of the mouth bar was aided by the overall gradient of the plate. In the lateral zones of flow convergence, typically on each side of the mouth bar, bedform trains were almost symmetrical (Fig. 11F), suggesting supercritical density flow conditions. In plan-view, the bedforms displayed a concentric geometry. Bedform trains evolved immediately downflow of deep scours, first showing symmetrical bedforms followed downslope by asymmetrical bedforms with a steeper stoss side (Fig. 11G). Internally, the asymmetrical bedforms displayed faint upflow dipping stratification (Fig. 11H). Downflow, the bedform train comprised two symmetrical bedforms followed by asymmetrical bedforms with steeper lee sides. During the runs the proximal bedforms were in-phase with the density flow interface. The authors' general interpretation of these features suggests a spatial pattern of supercritical stationary antidunes, followed immediately downstream by supercritical dunes (Fedele *et al.,* 2016), indicating decreasing Froude numbers in the downflow direction.

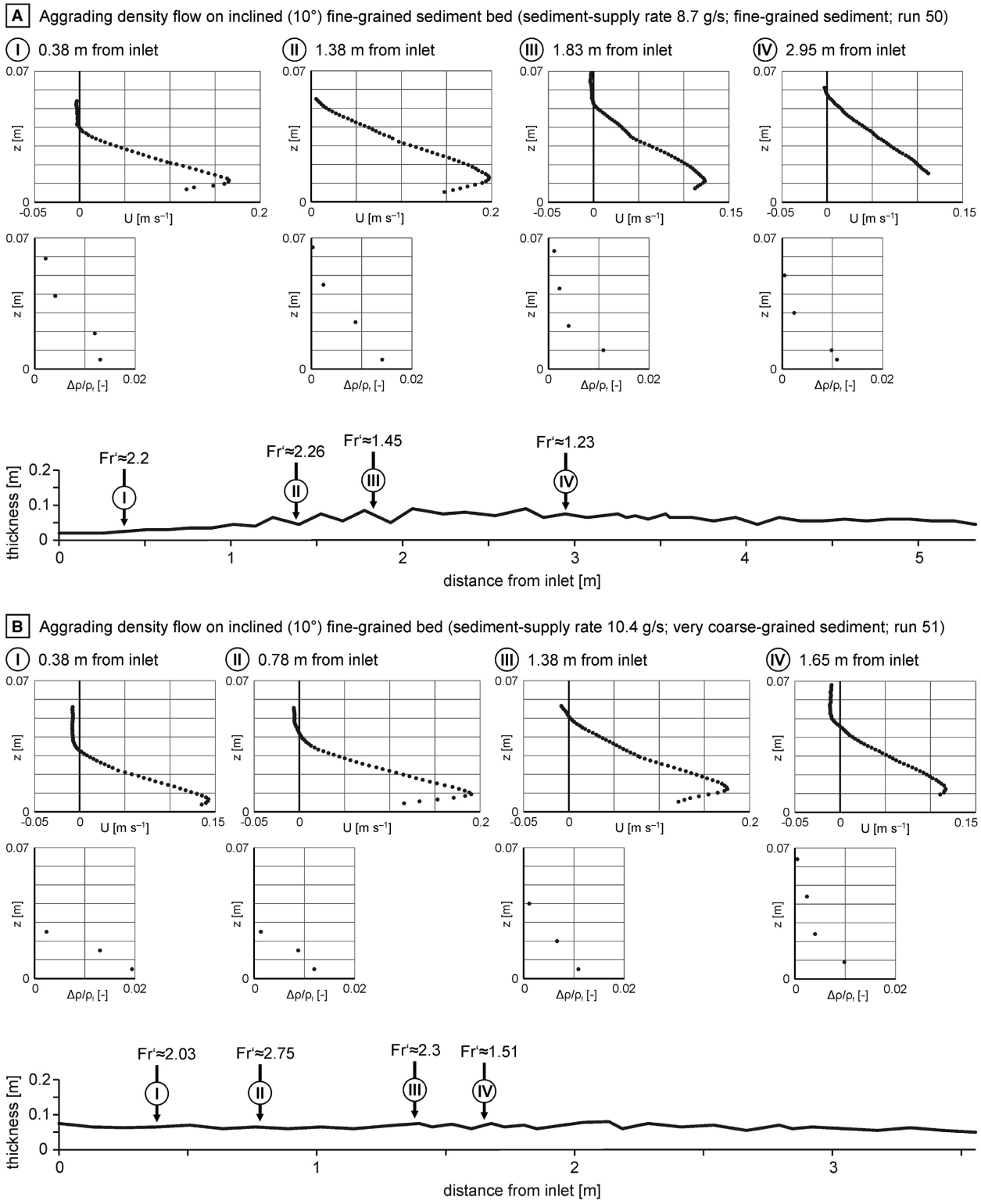

Fig. 12. Downflow evolution of density flows on inclined (10°) fine-grained sediment beds. Plots show the profiles of the velocity (U) and profiles of the fractional density difference ($\Delta\rho/\rho_f$) above the surface of the sediment bed (z). The locations of the measurements are indicated above thickness profiles of the sediment beds. (A) Discharge 0.63 l s^{-1}, initial fractional density difference 0.05, sediment-supply rate 8.7 g s^{-1}, fine-grained sediment (run 50). (B) Discharge 0.63 l s^{-1}, initial fractional density difference 0.05, sediment-supply rate 10.4 g s^{-1}, very coarse-grained sediment (run 51).

Density flows

Density flows expanded laterally from the inlet box, gravity-dominated from the start, and forming first a channel-like feature followed by a fan-shaped deposit built essentially by the growth and evolution of bedforms (Fig. 12). In the proximal parts of the expanding flows, after the channel, waveforms were large (10 to 30 cm wavelength), in-phase with the underlying deposit and clearly migrated upflow (antidunes). Measurements indicate an overall downflow decrease of the velocity, density and densimetric Froude numbers of the flows (Fig. 12). The flow velocities and densimetric Froude numbers are generally higher than those of density flows generated by jets under comparable conditions, remaining in general above unity (i.e. supercritical and around critical in the distal sections in some cases).

Fields of ripple-like bedforms formed within the first few minutes of the flow, extending from the inlet box to the toe of the slope. During the run time of the experiments (*ca* 1.5 to 2.0 h) 2 to 5 cm thick fan-shaped deposits were aggraded. The geometry of the deposits and the bedforms were closely related to the grain size of the supplied sediment. Fine-grained sediment led to the formation of a channel that extended for *ca* 1 m from the inlet box and widened downflow from 20.5 cm (width of the inlet box) to 36 cm. Low amplitude, rounded bedforms with wavelengths of 15 to 20 cm were deposited within the channel (antidunes). Downflow of the channel a fan was deposited, which was 4.6 m long, 1.2 m wide and had an aspect ratio (length/width) of 3.8. In the proximal part of the fan, crescentic, symmetrical to slightly upslope asymmetrical bedforms formed with wavelengths of 27 to 30 cm and wave heights of 2.5 to 3.0 cm. The bedforms migrated upslope and were in-phase with the density flow, with clear absence of internal hydraulic jumps (i.e. antidunes). The densimetric Froude number of the flow at the location of the bedforms ranged from 2.26 to 1.45. Downflow, bedforms became downflow asymmetrical with shorter wavelengths (10 to 12 cm) and lower wave heights (*ca* 1 cm), under flows with densimetric Froude number of *ca* 1.23. Because of the relatively high flow velocities and scaling with flow thickness, these asymmetrical bedforms are interpreted as supercritical dunes (i.e. not ripples). Flume experiments by Fedele *et al.* (2016) have shown that asymmetrical bedforms formed under sufficiently high flow velocities and bed-shear stress to move coarse-grained sediment generally represent supercritical dunes. Ripples, in contrast to dunes, do not interfere with the upper flow interface (Fedele *et al.,* 2016).

When very coarse-grained sediment was supplied, the density flow started to expand laterally and deposit sediments immediately at the inlet box, leading to the deposition of a fan (2.7 m long, 1.2 m wide, and with an aspect ratio length/width of 3.8) without an initial channel. Along the centre of the fan, crescentic symmetrical and asymmetrical bedforms evolved. These bedforms had wavelengths of 10 to 12 cm and heights of 0.8 to 1.5 cm, which both decreased downflow. In the proximal part of the deposit, the flow was in-phase with the bedforms, with densimetric Froude numbers computed from the measurements ranging from 2.75 to 1.51.

DISCUSSION

The transition from jets to density flows

One straightforward finding of this study is the clear zonation given by the scour–mouth-bar pair, resulting from a sharp transition between momentum-dominated flows inside the bar crest, and gravity-dominated flows from the mouth-bar crest and beyond. A second important finding supported by detailed measurements in all experimental runs is the absence of internal hydraulic jumps as transitional hydraulic elements. While these localized hydraulic features might be present in plane 2D wall-jets (Rajaratnam & Subramanyan, 1986; Long *et al.,* 1990, 1991), the new results support previous studies that suggest an absence of internal hydraulic jumps in expanding (3D) and submerged jets (Rajaratnam & Berry, 1977; Chiew & Lim, 1996; Ade & Rajaratnam, 1998). Free flow expansion and transformation in 3D wall-jets might preclude the formation of hydraulic jumps. Hydraulic jumps observed in 2D wall-jet experiments over non-erodible beds are typically induced by controlling the downstream boundary conditions in the flume through gates or obstacles, or experimental artifacts due to insufficient flume length (e.g. Rajaratnam & Subramanyam, 1986).

While horizontal dense wall jets behave like gravity-dominated density flows in some respects, the two flow types differ in terms of

driving mechanism and internal hydrodynamic processes, such as turbulent and buoyancy transport and the generation of turbulent stresses (Ljuboja & Rodi, 1981). The differences are more distinctive in the near-field of wall jets, where the flow is controlled by the continuous momentum input from the source.

Gravity-dominated density flows are flows with an interface and, as such, they respond to perturbations or obstacles imposed to the flow by adjusting their thickness and thus velocity. Like their subaerial counterparts, gravity-dominated density flows are characterized by hydraulic regimes that describe how the flow can transmit information of local flow changes through the generation of interfacial long-wavelength gravity waves (i.e. supercritical, critical and subcritical). An approaching supercritical flow can locally change to subcritical through a hydraulic jump, when the flow encounters a large enough obstacle and needs to gain enough potential energy to overcome it (hydraulic choke). In the case of jets, the continuous momentum input that drives the flow in the source proximity provides the energy necessary for the flow and its lower denser boundary layer to overcome the crest of the mouth bar. The geometry and dimensions of the scour are primarily a consequence of the momentum input and its dissipation through flow–bed interaction, whereas a true gravity-dominated density flow develops at and beyond the mouth-bar crest.

These findings have important sedimentological implications for developing recognition criteria and field interpretations. Previous outcrop-based sedimentological studies of jet deposits have commonly invoked hydraulic jumps to explain scouring and deposition in the zone of flow transition (Russell & Arnott, 2003; Hornung *et al.,* 2007; Winsemann *et al.,* 2009; Lang & Winsemann, 2013; Terlaky & Arnott, 2014; Terlaky *et al.,* 2016). These interpretations are likely based on extrapolation from observations and data from shallow water 2D jets, where hydraulic jumps are common (Rajaratnam & Subramanyan, 1986; Long *et al.,* 1990, 1991). Indeed, Fakhari & Kabiri-Samani (2017) showed that all dimensions of scours formed in experiments with subaerial hydraulic jumps were larger than the dimensions of scours in experiments where the transition from supercritical to subcritical flow did not involve hydraulic jumps. In all cases extrapolation from 2D jumps to 3D wall jets is not straightforward and caution should be applied.

In some experiments, the sediment was completely removed in the central part of the scour, which imposes an abrupt change on the boundary roughness and limits the free interaction of the flow with the bed, probably affecting the velocity field and jet dissipation. This might lead to transfer of some of the jet momentum farther downflow than in a setting allowing for unconstrained vertical expansion. However, the effect is probably minimal since the sediment-free areas in the centre of the scours were generally rather small. Furthermore, this does not affect the key observation that scour depth is controlled by the excess density of the incoming jets, resulting in the formation of deeper scours by denser flows. Denser incoming jets were observed to plunge from the orifice after scouring has started, favouring further erosion and scour deepening. The sediment is more effectively carried away from the scour and over the mouth bar by the density flow that evolves from the initial dense jet. Sediment bypass to downflow areas is especially intense on sloping beds and may result in the formation of very low mouth bars (Fig. 9E). The transition from bed degradation to aggradation in settings with sloping beds and dense flows occurred at distances from the orifice (*ca* 1.1 m) that exceeded the lengths of the mouth bars observed in other experiments (Fig. 9F). Experiments with density flows that expanded from an inlet box generated bedforms that were very similar to those generated by density flows that were derived from a jet. Antidune trains that formed in the density-flow experiments had longer wavelengths compared with those formed in jet experiments, most likely due to the higher velocity of density flows. Jets are decelerated in the initial expansion state and reacceleration occurs after the full transition to density flows.

In summary, basic flow processes in the near-field regions of an expanding wall jet driven by the momentum efflux are different from far-field gravity-dominated interfacial flow, such as open-channel or density/turbidity flows with a well-developed interface. In the experiments with stratified jets running over fixed horizontal beds hydraulic jumps are absent at the transition from momentum-dominated jets to gravity-dominated density flows. In contrast, the dynamics controlling flow transformation are different and include complex flow recirculation, pulsating bursts and waves and flow splitting within the scour. On fixed beds the mechanism appears more subtle and gradual due to the absence of

scouring. In the near-field it is not clear whether there is an interface and consequently the concept of flow criticality may not apply.

Flow behaviour over fixed versus sediment beds

The observation of bedform fields in the experiments reflects differences in flow and sediment transport associated with changes in experimental set-up. These include fixed versus evolving beds, initial pure jets versus density flows and sediment injected versus sediment free flow at the inlet. In sediment-free (non-morphodynamic) settings the measured velocity profiles revealed simple and expected flow patterns, primarily flow deceleration, thickening due to mixing and expansion and frictional effects (Fig. 3). In contrast, the morphodynamic experiments (non-aggrading and aggrading), display far more complex patterns. Velocity profiles measured during runs with sediment include the formation of recirculation cells within the scours and reacceleration of the flows on the lee sides of the mouth bars (Figs 4 and 5). Parts of the flow remained in the scour as stationary, recirculating turbulent dense fluid until it was displaced outward by pulsating bursts or waves in some cases, clearly as consequence of complex flow interactions driven by the discharge of the jets, momentum and density influx interacting with the flow induced scour topography. These processes led to a strong frontal and lateral spreading of the density flow and sediment distribution over the mouth bar and further downflow.

In experiments on fixed beds, stratified jets evolved into purely gravity-dominated spatially evolving density flows after a sufficient distance from the orifice was reached. In contrast, scouring and mouth-bar aggradation on sediment beds indicated more clearly the momentum-dominated near-field and allowed for the transition and formation of downslope moving density flows downflow at the mouth-bar crest. Velocity profiles measured on the lee sides of the mouth bars show significant acceleration induced by the topographic slope of these features. The reacceleration of the density flows was sufficient to notably increase the bedload-transport rates, evidenced by the formation of bedform trains on the lee-sides of the mouth bars and also on the horizontal sediment bed beyond the base of the mouth bar (Figs 4 and 5). Upflow, where the recently developed density flows were stronger, antidune and dune-like bedforms prevailed, all developing under predominantly supercritical flow conditions, as indicated by flow measurements. Farther downflow, ripples prevailed due to lower flow velocities.

Because the suspended sediment concentration was not measured in this study, it is not clear whether the density flows were self-accelerating in the sense of Sequeiros *et al.* (2009) or if flow acceleration was purely slope controlled. Downflow acceleration along a decreasing mouth-bar slope (measurements II and III in Fig. 5A) and the visual observation of suspended sediment may indicate that some density flows are self-accelerating.

Implications for the depositional record

In general, the experiments can be considered as analogue representations of natural systems based on similar hydraulic and transport regimes that allow for the occurrence of similar processes. However, due to the large geometrical scaling ratio, the experimental conditions cannot simply be upscaled to natural systems by formal scaling laws. The focus of this study is the near-field where an important aspect of the free (channel) and forced (pipe) jets is the creation of shear layers, and increase in turbulence scales and intensity at the orifice. In some geological settings, like subaqueous ice-contact fans, jets are more likely follow the experimental geometry closely. Other settings like stratified supercritical density flows and turbidity currents confined in channels on submarine fans also produce a jet-like geometry at the channel terminus and wall-jet analogies have been applied (e.g. Hamilton *et al.,* 2015, 2017). However, channelized wall jets and forced jets are different as discussed earlier.

Subaqueous ice-contact fans

Subaqueous ice-contact fans deposited by meltwater released at the grounding line of a glacier represent an ideal field example of deposition by submerged wall jets as the subglacial conduit has the potential to produce large values of excess inertia. The deposits represent the mouth bars of the glacigenic jets (Powell, 1990; Winsemann *et al.,* 2009; Dowdeswell *et al.,* 2015). Experimental results reported herein indicate that coarse-grained sediment is commonly transported as bedload sheets from the orifice, building a strongly aggradational mouth bar. Large-scale scours (1 to 3 km long, *ca* 1 km wide and

7 to 25 m deep) observed at the base of subaqueous ice-contact fans are consistent with the scours formed by the experimental jets in this study (Winsemann *et al.,* 2009; Lang & Winsemann, 2013). Smaller-scale scours with locally very steep walls (several decimetres to tens of metres wide, several decimetres to metres deep) in gravelly and sandy subaqueous ice-contact fan successions were interpreted as related to hydraulic jumps (e.g. Russell & Arnott, 2003; Hornung *et al.,* 2007; Winsemann *et al.,* 2009; Lang & Winsemann, 2013). The present results offer alternative explanations for the cases of these steep-walled scours, because hydraulic jumps were absent in the jet experiments reported here, including: (i) scouring by impinging jet-derived eddies; (ii) chute formation by slope failures; and (iii) scouring by the density flows that develop on the lee of mouth bars. Proximal subaqueous ice-contact successions comprise wide (up to 25 m), shallow (0.3 to 3.0 m) lenticular scours that are organized into upslope-dipping packages (Winsemann *et al.,* 2009; Lang *et al.,* 2020) and may represent field examples for scouring by the impingement of jet-derived eddies on the inner margin of a mouth bar. Chutes related to slope failures are well-known from the, commonly much steeper, foreset slopes of Gilbert-type deltas (Postma & Cruickshank, 1988; Lønne, 1995; Breda *et al.,* 2007; Winsemann *et al.,* 2018). In the experiments, impingement by eddies was observed to trigger slope failures on both the stoss and lee sides of the mouth bar. The sediment was partly re-entrained by eddies from the jet and partly deposited in the scour or at the base of the mouth bar. In subaqueous ice-contact fans such processes may cause the deposition of highly scoured coarse-grained deposits, which are commonly interpreted as deposits of hyperconcentrated flows (cf. Russell & Arnott, 2003; Hornung *et al.,* 2007; Winsemann *et al.,* 2009; Lang *et al.,* 2017).

The density flows observed in the experiments formed small-scale sours and bedform trains downflow of the mouth bar (Fig. 11). The bedform trains commonly passed laterally from antidunes into dunes. Sand-rich deposits related to isolated hydraulic jumps, antidunes and (humpback) dunes in subaqueous ice-contact fans are interpreted as deposited by supercritical density flows on the lee side of the mouth bar (cf. Lang *et al.,* 2017). The characteristic association of antidune and humpback-dune deposits in sandy ice-contact fan successions (Lang & Winsemann, 2013) may relate to the lateral transitions between bedforms as they were observed in the experiments.

Deep water depositional systems

The applicability of near-field momentum-dominated jet processes on expanding density flows in deep water depositional systems is more equivocal but the experiments offer some important insights. Examples of deep water depositional environments where results from the experimental wall jets can be applied more directly include submarine fans, lobes and crevasse splays, which record flow expansion from the mouths of canyons, distributary channels and crevasse channels, respectively (Beaubouef *et al.,* 2003; Alexander *et al.,* 2008; Terlaky & Arnott, 2014; Terlaky *et al.,* 2016). Pipe flows produce a more rapid jet transition since in channels the flow can interact with the ambient water at the upper boundary of the flow upstream of the channel mouth. Nevertheless, channelized density flows characterized by a high momentum (for example, high-velocity flows on steep slopes) do display jet-like behaviour upon flow expansion (Baas *et al.,* 2004; Alexander *et al.,* 2008). Supercritical density flows, which are defined by the dominance of inertia over gravity forces, have been observed to display jet-like behaviour when expanding from a confinement (Hamilton *et al.,* 2015, 2017). Furthermore, the behaviour of an expanding density flow is affected by the geometry of the confinement. Narrow and deep channels will contribute to a more jet-like behaviour of the expanding flow (Alexander *et al.,* 2008).

A prominent example of deep water settings characterized by expanding density flows are channel-lobe transition zones (CLTZs). CLTZs comprise radially spreading fields of scours and bedforms that connect downdip from the channel mouth to the proximal lobe (Mutti & Normark, 1987; Wynn *et al.,* 2002; Macdonald *et al.,* 2011; Hofstra *et al.,* 2015, 2018; Brooks *et al.,* 2018). The lengths of CLTZs range from few kilometres to >100 km. Individual scours are 20 to 3000 m long, 20 to 3000 m wide, <1 to 300 m deep, and typically become smaller and more isolated in downdip direction (Wynn *et al.,* 2002; Macdonald *et al.,* 2011). Scouring is commonly attributed to increased turbulence related to hydraulic jumps triggered at the slope break (Komar, 1971; Mutti & Normark, 1987; Wynn *et al.,* 2002). To trigger hydraulic jumps, a slope break or an obstacle that induces hydraulic

choking is required (Komar, 1971; Garcia & Parker, 1989; Hamilton *et al.,* 2015, 2017). Turbulence related to expanding jets provides another explanation for the intense scouring by expanding flows in CLTZs, offering several advantages over the hydraulic-jump model. The jet model can also explain scouring by expanding subcritical flows, where hydraulic jumps can be excluded. Alternatively, scouring in a CLTZ has been explained by flow relaxation (Pohl *et al.,* 2019). The loss of confinement triggers internal flow deformation and a lowering of the velocity maximum of the flow, which increases the velocity gradient in the basal flow despite overall flow deceleration, finally resulting in enhanced shear velocity and erosion (Pohl *et al.,* 2019). In the present experiments, however, scouring in the near-field zone of the jet was clearly caused by turbulent eddies at the free boundaries of the jet. A lowering of the velocity maximum, which may be attributed to flow relaxation as described by Pohl *et al.* (2019), occurred farther downflow after the transition to a more gravity driven-density flow (Figs 4B and 6). Sediment movement observed in these parts of the flows can probably be explained by enhanced shear velocity due to flow relaxation. It is interesting to note that a lowering of the velocity maximum was not observed in the density-flow experiments (Fig. 12).

Hamilton *et al.* (2015, 2017) showed in experiments with density flows that the early morphodynamic stage of expanding supercritical flows displays jet-like behaviour due to the high momentum of the incoming flow. In this early stage, prograding frontal splays (mouth bars) are deposited, which grow and subsequently induce a hydraulic choke and trigger hydraulic jumps (Hamilton *et al.,* 2015, 2017). Outcrop studies by Terlaky & Arnott (2014) interpreted mud-prone sandstones as avulsion splays related to erosion of the muddy seafloor by jets during the earliest stage of avulsion. These avulsion-splay deposits are overlain by clean sandstones, representing the actual lobe deposits (Terlaky & Arnott, 2014).

Forced rapid hydraulic transitions like jets and jumps are common in experiments but are problematic if the objective is to observe channel morphodynamics like distributary channel formation, self-organization and avulsion (Yu *et al.,* 2006; Cantelli *et al.,* 2011; Fernandez *et al.,* 2014). Mouth-bar formation in these experiments is usually regarded as an artifact of the experimental configuration (Yu *et al.,* 2006; Fernandez *et al.,* 2014), because such experiments are designed to drop a minimum of sediment at the inlet jet and to transmit the sediment to the region of interest more distally as suspended load. However, the experiments here were designed specifically to investigate coarse-grained bedload sediment and mouth-bar growth while fine-grained sediment led to bypass, even for high rates of the sediment-supply (Fig. 11A and F). Examples of deep water prograding mouth bars are known from expanding very coarse-grained turbidity currents (Mutti, 1977; Mutti & Normark, 1987; Gamberi *et al.,* 2014; Ferry *et al.,* 2015; Grosheny *et al.,* 2015) and chute-mouth lobes in Gilbert-type deltas (Postma & Cruickshank, 1988; Breda *et al.,* 2007).

The distal parts of CLTZs are characterized by concentric bedform trains that are commonly referred to as sediment waves (Wynn *et al.,* 2002). The concentric early-stage bedforms formed by the experimental jets strongly resemble such concentric sediment-wave fields (Figs 7A and 8B to D). Based on their sedimentary facies, deposits of the CLTZ have been attributed to both subcritical (e.g. Brooks *et al.,* 2018; Hofstra *et al.,* 2018) and supercritical flows (e.g. Onishi *et al.,* 2018; Postma & Kleverlaan, 2018; Postma *et al.,* 2020). This corresponds to the jet experiments, where both subcritical and supercritical flow conditions were responsible for the formation of early-stage concentric bedforms. As mentioned earlier, density-flow conditions depend on the bed slope and excess density, primarily, with supercritical flows being promoted by not only steeper slopes and denser flows but also by flow thinning as a result of flow expansion, at least under the observed laboratory conditions.

CONCLUSIONS

The experiments show the evolution from momentum-dominated jets to gravity-dominated density flows. Bedform successions are formed by both the initial jets and the density flows. All experimental jet deposits comprise early-stage bedforms, scours and mouth bars. Gravity-dominated processes rapidly take over the control on the morphodynamic evolution of the flow and are responsible for deposition on the lee side of the mouth bar and beyond. The mouth-bar crest can thus be considered as the transition between momentum-dominated and gravity-dominated

processes. The experiments indicate that hydraulic jumps are absent in this transition, but instead, complex flow recirculations and large-scale turbulent eddies, bursts and waves, are responsible for the development and maintenance at the final stages of equilibrium of the scour and associated mouth bar.

Stratified (dense) jets with small excess density produce scours with larger aspect ratios (length versus width). Conversely, the scours are deeper when denser flows were input. Scours formed by the entrainment of sediment by turbulent eddies, and were associated with the intense efflux momentum and related turbulent dissipation. The entrained sediment was typically flushed out of the scour to build a mouth bar around the scour margin. The observations and results suggest that the height and steepness of the mouth bar and bedforms were primarily controlled by the grain size and flow conditions over the mouth bar, with coarser-grained sediment causing the formation of higher and steeper bars and bedforms.

Bedform trains that developed beyond the mouth-bar crest were observed to result from density flows triggered after the transition from momentum-dominated to gravity-dominated flow. Bedform formation and type was controlled by the bed slope, sediment grain size and sediment supply. The supply of coarse-grained sediment led to excessive growth of the mouth bar, thus inducing lateral flow diversions from the scour and the development of lateral density flows, with characteristic bedforms representing successions of antidunes and then dunes, mostly under supercritical flow conditions. When finer-grained sediment was supplied, the mouth bar remained low and bedform trains evolved along the centreline of the flow. These bedforms also showed a transition from antidune-like to dune-like, after flows clearly transitioned to gravity-dominated conditions. All measurements confirmed that these flows were supercritical density flows.

Subaqueous ice-contact fans deposited at the grounding line of glaciers represent ideal field examples of deposition by momentum-dominated, submerged wall jets. Proximal subaqueous ice-contact fan deposits represent the mouth bars of glacigenic jets. Internal scouring of mouth-bar deposits may be related to impinging jet eddies generated by the expanding glacigenic jet, leading to scouring. Distal finer-grained fan successions are deposited by the density flows that evolved from the initial jets. Typical successions, including antidunes to dunes (symmetrical to asymmetrical, supercritical bedforms) were most commonly observed in the experiments, and might therefore represent a key component for interpretation criteria of these particular environments, because these characteristic bedform successions have been observed also in the field in glacigenic, jet-outflow-related deposits, but rarely occur in such close connection in more typical channel-lobe transition zone deposits of turbidity currents.

While the distinction between momentum-dominated expanding jets and submarine channel flow carrying gravity-dominated turbidity (or density) flows must be kept in mind, the bedform successions formed by the experimental jets, particularly those related to the gravity-dominated flows triggered over the mouth-bar crest, strongly resemble those observed in some deep water channel-lobe transition zones. Thick prograding mouth bars, which were a characteristic sedimentary feature in these experimental jet deposits, are rare in deep water settings. Concentric bedform trains were observed in the experiments, developing particularly in areas where flows have transitioned to gravity-dominated (i.e. just after the scour). Analogous configurations are known from modern deep water settings, for example channel-lobe transition zones. It is not clear whether direct analogies can be drawn between proximal channel-lobe transition zones and near-field jet morphodynamics, at least from a purely flow-related view, because CLTZs involve gravity-dominated flows, whereas jets are characterized by a momentum-dominated input in the near-field. However, the nature of deposits and associated bedforms might be more similar once flows have transitioned to gravity-dominated (i.e. beyond the mouth bar).

ACKNOWLEDGEMENTS

This study was funded by Leibniz Universität Hannover ('Wege in die Forschung' – postdoc-funding scheme; Grant II-05-2014-05) and the German Research Foundation (DFG; Grant LA 4422/1-1). We are grateful for the support by ExxonMobil Upstream Research Company for providing access to the experimental facility and supplying the consumables for the experiments. J. Winsemann and the members of the ExxonMobil Upstream Research Company's Process Stratigraphy team are thanked for discussion. Constructive reviews by F. Pohl and an anonymous reviewer are highly appreciated. The

editorial team (A. Slootman, M. Cartigny, A. Normandeau, D. Ventra and S. Hubbard) of the *Sedimentology* special issue is thanked for inviting us to contribute this paper. Open access funding was provided by project DEAL.

DATA AVAILABILITY STATEMENT

The data that support the findings of this study are available from the corresponding author upon reasonable request.

REFERENCES

Ade, F. and **Rajaratnam, N.** (1998) Generalized study of erosion by circular horizontal turbulent jets. *J. Hydraul. Res.*, **36**, 613–636.

Ahmed, S., **Bhattacharya, J.P.**, **Garza, D.E.** and **Li, Y.** (2014) Facies architecture and stratigraphic evolution of a river-dominated delta front, Turonian Ferron Sandstone, Utah, USA. *J. Sed. Res.*, **84**, 97–121.

Alexander, J., **McLelland, S.J.**, **Gray, T.E.**, **Vincent, C.E.**, **Leeder, M.R.** and **Ellett, S.** (2008) Laboratory sustained turbidity currents form elongate ridges at channel mouths. *Sedimentology*, **55**, 845–868.

Aquino, C.D., **Buso, V.V.**, **Faccini, U.F.**, **Milana, J.P.** and **Paim, P.S.G.** (2016) Facies and depositional architecture according to a jet efflux model of a late Paleozoic tidewater grounding-line system from the Itararé Group (Paraná Basin), southern Brazil. *J. S. Am. Earth Sci.*, **67**, 180–200.

Baas, J.H., **Van Kesteren, W.** and **Postma, G.** (2004) Deposits of depletive high-density turbidity currents: a flume analogue of bed geometry, structure and texture. *Sedimentology*, **51**, 1053–1088.

Baines, P.G. (1995) *Topographic Effects in Stratified Flows*. Cambridge University Press, Cambridge, 482 pp.

Baines, P.G. (2002) Two-dimensional plumes in stratified environments. *J. Fluid Mech.*, **471**, 315–337.

Bates, C.C. (1953) Rational theory of delta formation. *AAPG Bull.*, **37**, 2119–2162.

Beaubouef, R.T., **Van Wagoner, J.C.** and **Adair, N.L.** (2003) Ultra-high resolution 3-D characterization of deep-water deposits - II: Insights into the evolution of a submarine fan and comparisons with river deltas. Search and Discovery Article #40085.

Breda, A., **Mellere, D.** and **Massari, F.** (2007) Facies and processes in a Gilbert-delta-filled incised valley (Pliocene of Ventemiglia, NW Italy). *Sed. Geol.*, **200**, 31–55.

Brooks, H.L., **Hodgson, D.M.**, **Brunt, R.L.**, **Peakall, J.**, **Hofstra, M.** and **Flint, S.S.** (2018) Deep-water channel-lobe transition zone dynamics: processes and depositional architecture, an example from the Karoo Basin, South Africa. *GSA Bull.*, **130**, 1723–1746.

Cantelli, A., **Pirmez, C.**, **Johnson, S.** and **Parker, G.** (2011) Morphodynamic and stratigraphic evolution of self-channelized subaqueous fans emplaced by turbidity currents. *J. Sed. Res.*, **81**, 233–247.

Chiew, Y.M. and **Lim, S.Y.** (1996) Local scour by a deeply submerged horizontal circular jet. *J. Hydraul. Eng.*, **122**, 529–532.

Chu, V.H. and **Baddour, R.E.** (1984) Turbulent gravity-stratified shear flows. *J. Fluid Mech.*, **138**, 353–378.

Craft, T.J. and **Launder, B.E.** (2001) On the spreading mechanism of the three-dimensional turbulent wall jet. *J. Fluid Mech.*, **435**, 305–326.

Daniller-Varghese, M.S., **Kim, W.** and **Mohrig, D.C.** (2020) The effect of flood intermittency on bifurcations in fluviodeltaic systems: experiment and theory. *Sedimentology*, **67**, 3055–3066. https://doi.org/10.1111/sed.12732

Dowdeswell, J.A., **Hogan, K.A.**, **Arnold, N.S.**, **Mugford, R.I.**, **Wells, M.**, **Hirst, J.P.P.** and **Decalf, C.** (2015) Sediment-rich meltwater plumes and ice-proximal fans at the margins of modern and ancient tidewater glaciers: observations and modelling. *Sedimentology*, **62**, 1665–1692.

Ellison, T.H. and **Turner, J.S.** (1959) Turbulent entrainment in stratified flows. *J. Fluid Mech.*, **6**, 423–448.

Fakhari, Z. and **Kabiri-Samani, A.** (2017) Scour in the transition from super- to subcritical flow without a hydraulic jump. *J. Hydraul. Res.*, **55**, 470–479.

Fedele, J.J., **Hoyal, D.C.**, **Barnaal, Z.**, **Tulenko, J.** and **Awalt, S.** (2016) Bedforms created by gravity flows. In: *Autogenic Dynamics in Sedimentary Systems* (Eds Budd, D., Hajek, E. and Purkis, S.), *SEPM Spec. Publ.*, **106**, 95–121, Tulsa.

Fernandez, R.L., **Cantelli, A.**, **Pirmez, C.**, **Sequeiros, O.** and **Parker, G.** (2014) Growth patterns of subaqueous depositional channel lobe systems developed over a basement with a downdip break in slope: laboratory experiments. *J. Sed. Res.*, **84**, 168–182.

Ferry, S., **Grosheny, D.**, **Backert, N.** and **Atrops, F.** (2015) The base-of-slope carbonate breccia system of Céüse (Tithonian, SE France): occurrence of progradational stratification in the head plug of coarse granular flow deposits. *Sed. Geol.*, **317**, 71–86.

Fidolini, F. and **Ghinassi, M.** (2016) Friction-and inertia-dominated effluents in a lacustrine, river-dominated deltaic succession (Pliocene Upper Valdarno Basin, Italy). *J. Sed. Res.*, **86**, 1083–1101.

Fischer, H.B., **List, J.E.**, **Koh, C.R.**, **Imberger, J.** and **Brooks, N.H.** (1979) *Mixing in Inland and Coastal Waters*. Academic Press, New York, 483 pp.

Gamberi, F., **Rovere, M.**, **Mercorella, A.** and **Leidi, E.** (2014) The influence of a lateral slope on turbidite lobe development on a modern deep-sea slope fan (Villafranca deep-sea fan, Tyrrhenian Sea). *J. Sed. Res.*, **84**, 475–486.

Garcia, M. and **Parker, G.** (1989) Experiments on hydraulic jumps in turbidity currents near a canyon-fan transition. *Science*, **245**, 393–396.

Grosheny, D., **Ferry, S.** and **Courjault, T.** (2015) Progradational patterns at the head of single units of base-of-slope, submarine granular flow deposits ("Conglomérats des Gâs", Coniacian, SE France). *Sed. Geol.*, **317**, 102–115.

Hamilton, P., **Gaillot, G.**, **Strom, K.**, **Fedele, J.** and **Hoyal, D.C.** (2017) Linking hydraulic properties in supercritical submarine distributary channels to depositional-lobe geometry. *J. Sed. Res.*, **87**, 935–950.

Hamilton, P.B., **Strom, K.B.** and **Hoyal, D.C.** (2015) Hydraulic and sediment transport properties of autogenic avulsion cycles on submarine fans with supercritical distributaries. *J. Geophys. Res. Earth Surf.*, **120**, 1369–1389.

Hofstra, M., **Hodgson, D.M.**, **Peakall, J.** and **Flint, S.S.** (2015) Giant scour-fills in ancient channel-lobe transition zones: formative processes and depositional architecture. *Sed. Geol.*, **329**, 98–114.

Hofstra, M., **Peakall, J.**, **Hodgson, D.M.** and **Stevenson, C.J.** (2018) Architecture and morphodynamics of subcritical sediment waves in an ancient channel-lobe transition zone. *Sedimentology*, **65**, 2339–2367.

Hornung, J.J., **Asprion, U.** and **Winsemann, J.** (2007) Jet-efflux deposits of a subaqueous ice-contact fan, glacial Lake Rinteln, northwestern Germany. *Sed. Geol.*, **193**, 167–192.

Hoyal, D.C.J.D., **Van Wagoner, J.C.**, **Adair, N.L.**, **Deffenbaugh, M.**, **Li, D.**, **Sun, T.**, **Huh, C.** and **Griffin, D.E.** (2003) Sedimentation from Jets: A Depositional Model for Clastic Deposits of all Scales and Environments. *Search and Discovery Article 40082* (Online-Journal; AAPG/Datapages, Inc., 1444 South Boulder, Tulsa, OK, 74119, USA).

Jirka, G.H. (2004) Integral model for turbulent buoyant jets in unbounded stratified flows. Part I: single round jet. *Environ. Fluid Mech.*, **4**, 1–56.

Komar, P.D. (1971) Hydraulic jumps in turbidity currents. *GSA Bull.*, **82**, 1477–1487.

Lang, J., **Le Heron, D.P.**, **van den Berg, J.H.** and **Winsemann, J.** (2020) Bedforms and sedimentary structures related to supercritical flows in glacigenic settings. *Sedimentology*. https://doi.org/10.1111/sed.12776

Lang, J., **Sievers, J.**, **Loewer, M.**, **Igel, J.** and **Winsemann, J.** (2017) 3D architecture of cyclic-step and antidune deposits in glacigenic subaqueous fan and delta settings: integrating outcrop and ground-penetrating radar data. *Sed. Geol.*, **362**, 83–100.

Lang, J. and **Winsemann, J.** (2013) Lateral and vertical facies relationships of bedforms deposited by aggrading supercritical flows: from cyclic steps to humpback dunes. *Sed. Geol.*, **296**, 36–54.

Launder, B.E. and **Rodi, W.** (1983) The turbulent wall jet measurements and modeling. *Annu. Rev. Fluid Mech.*, **15**, 429–459.

List, E.J. (1982) Turbulent jets and plumes. *Annu. Rev. Fluid Mech.*, **14**, 189–212.

Ljuboja, M. and **Rodi, W.** (1981) Prediction of horizontal and vertical turbulent buoyant wall jets. *J. Heat Transfer*, **103**, 343–349.

Long, D., **Rajaratnam, N.**, **Steffler, P.M.** and **Smy, P.R.** (1991) Structure of flow in hydraulic jumps. *J. Hydraul. Res.*, **29**, 207–218.

Long, D., **Steffler, P.M.** and **Rajaratnam, N.** (1990) LDA study of flow structure in submerged hydraulic jump. *J. Hydraul. Res.*, **28**, 437–460.

Lønne, I. (1995) Sedimentary facies and depositional architecture of ice-contact glaciomarine systems. *Sed. Geol.*, **98**, 13–43.

Macdonald, H.A., **Wynn, R.B.**, **Huvenne, V.A.**, **Peakall, J.**, **Masson, D.G.**, **Weaver, P.P.** and **McPhail, S.D.** (2011) New insights into the morphology, fill, and remarkable longevity (>0.2 my) of modern deep-water erosional scours along the northeast Atlantic margin. *Geosphere*, **7**, 845–867.

Mutti, E. (1977) Distinctive thin-bedded turbidite facies and related depositional environments in the Eocene Hecho Group (South-Central Pyrenees, Spain). *Sedimentology*, **24**, 107–131.

Mutti, E. and **Normark, W.R.** (1987) Comparing examples of modern and ancient turbidite systems: problems and concepts. In: *Marine Clastic Sedimentology* (Eds Leggett, J.K. and Zuffa, G.G.), pp. 1–38.Graham and Trotman, London.

Onishi, Y., **Takii-Kawakami, K.**, **Abe, H.** and **Ishihara, Y.** (2018) Facies distribution in sediment-gravity-flow deposits constructing sediment waves: an outcrop example of forearc basin fills, Neogene Aoshima Formation, southwest Japan. *J. Sed. Res.*, **88**, 260–275.

Pohl, F., **Eggenhuisen, J.T.**, **Tilston, M.** and **Cartigny, M.J.B.** (2019) New flow relaxation mechanism explains scour fields at the end of submarine channels. *Nature Comm.*, **10**, 1–8.

Postma, G. and **Cruickshank, C.** (1988) Sedimentology of a late Weichselian to Holocene terraced fan delta, Varangerfjord, northern Norway. In: *Fan Deltas: Sedimentology and Tectonic Settings* (Eds Nemec, W. and Steel, R.J.), pp. 144–157.Blackie, London.

Postma, G. and **Kleverlaan, K.** (2018) Supercritical flows and their control on the architecture and facies of small-radius sand-rich fan lobes. *Sed. Geol.*, **364**, 53–70.

Postma, G., **Lang, J.**, **Hoyal, D.C.**, **Fedele, J.J.**, **Demko, T.**, **Abreu, V.** and **Pederson, K.H.** (2020) Reconstruction of bedform dynamics controlled by supercritical flow in the channel-lobe transition zone of a deep-water delta (Sant Llorenç del Munt, NE Spain, Eocene). *Sedimentology*. https://doi.org/10.1111/sed.12735

Powell, R.D. (1990) Glacimarine processes at grounding-line fans and their growth to ice-contact deltas. In: *Glacimarine Environments: Processes and Sediments* (Eds Dowdeswell, J.A. and Scourse, J.D.), *Geol. Soc. Spec. Pub.*, **53**, 53–73, Geological Society, London.

Rajaratnam, N. and **Berry, B.** (1977) Erosion by circular turbulent wall jets. *J. Hydraul. Res.*, **15**, 277–289.

Rajaratnam, N. and **Subramanyam, S.** (1986) Plane turbulent denser wall jets and jumps. *J. Hydraul. Res.*, **24**, 281–296.

Roberts, P.J., **Maile, K.** and **Daviero, G.** (2001) Mixing in stratified jets. *J. Hydraul. Eng.*, **127**, 194–200.

Russell, H.A.J. and **Arnott, R.W.C.** (2003) Hydraulic jump and hyperconcentrated-flow deposits of a glacigenic subaqueous fan: Oak Ridges Moraine, Southern Ontario, Canada. *J. Sed. Res.*, **73**, 887–905.

Sequeiros, O.E. (2012) Estimating turbidity current conditions from channel morphology: a Froude number approach. *J. Geophys. Res.*, **117**, C04003.

Sequeiros, O.E., **Naruse, H.**, **Endo, N.**, **Garcia, M.H.** and **Parker, G.** (2009) Experimental study on self-accelerating turbidity currents. *J. Geophys. Res. Oceans*, **114**, C5.

Strom, K. and **Keyvani, A.** (2011) An explicit full-range settling velocity equation for mud flocs. *J. Sed. Res.*, **81**, 921–934.

Terlaky, V. and **Arnott, R.W.C.** (2014) Matrix-rich and associated matrix-poor sandstones: avulsion splays in slope and basin-floor strata. *Sedimentology*, **61**, 1175–1197.

Terlaky, V., **Rocheleau, J.** and **Arnott, R.W.C.** (2016) Stratal composition and stratigraphic organization of stratal elements in an ancient deep-marine basin-floor succession, Neoproterozoic Windermere Supergroup, British Columbia, Canada. *Sedimentology*, **63**, 136–175.

Tollmien, W. (1926) Berechnung turbulenter Ausbreitungsvorgänge. *Z. Angew. Math. Mech.*, **6**, 468–478.

Turner, J.S. (1986) Turbulent entrainment: the development of the entrainment assumption, and its application to geophysical flows. *J. Fluid Mech.*, **173**, 431–471.

Wellner, R., **Beaubouef, R.**, **Van Wagoner, J.C.**, **Roberts, H.** and **Sun, T.** (2005) Jet-plume depositional bodies - the primary building blocks of Wax Lake Delta. *Trans. Gulf Coast Assoc. Geol. Soc.*, **55**, 867–909.

Winsemann, J., **Hornung, J.J.**, **Meinsen, J.**, **Asprion, U.**, **Polom, U.**, **Brandes, C.**, **Bußmann, M.** and **Weber, C.** (2009) Anatomy of a subaqueous ice-contact fan and delta complex, Middle Pleistocene, NW Germany. *Sedimentology*, **56**, 1041–1076.

Winsemann, J., **Lang, J.**, **Polom, U.**, **Loewer, M.**, **Igel, J.**, **Pollolk, L.** and **Brandes, C.** (2018) Ice-marginal forced-regressive deltas in glacial lake basins: geomorphology, facies variability and large-scale depositional architecture. *Boreas*, **47**, 973–1002.

Wright, L.D. (1977) Sediment transport and deposition at river mouths: a synthesis. *Geol. Soc. Am. Bull.*, **88**, 857–868.

Wu, S. and **Rajaratnam, N.** (1995) Free jumps, submerged jumps and wall jets. *J. Hydraul. Res.*, **33**, 197–212.

Wynn, R.B., **Kenyon, N.H.**, **Masson, D.G.**, **Stow, D.A.V.** and **Weaver, P.P.E.** (2002) Characterization and recognition of deep-water channel-lobe transition zones. *AAPG Bull.*, **86**, 1441–1462.

Yu, B., **Cantelli, A.**, **Marr, J.**, **Pirmez, C.**, **O'Byrne, C.** and **Parker, G.** (2006) Experiments on self-channelized subaqueous fans emplaced by turbidity currents and dilute mudflows. *J. Sed. Res.*, **76**, 889–902.

Manuscript received 30 January 2020; revision accepted 17 February 2021

Supporting Information

Additional information may be found in the online version of this article:

Video S1. Video of a typical stratified aggrading jet on a horizontal sediment bed (run 33; discharge 0.63 l s^{-1}; initial flow density 1.01 kg l^{-1}; sediment-supply rate 2.2 g s^{-1}; Fr′ = 4.02).

Video S2. Video of a stratified aggrading jet on a sloping (10°) sediment bed (run 47; discharge 0.63 l s^{-1}; initial flow density 1.06 kg l^{-1}; sediment-supply rate 8.7 g s^{-1}; Fr′ = 1.99). Note the formation of in-phase bedforms.

Video S3. Video of an aggrading density flow on a sloping (10°) sediment bed (run 50; discharge 0.63 l s^{-1}; initial flow density 1.05 kg l^{-1}; sediment-supply rate 8.7 g s^{-1}). Note the formation of in-phase bedforms, which have longer wavelengths than those formed by density flows developed from a jet.